



Incorporating mortality shocks into a multi-population mortality model

by

A.S. Panah (SNR: 2022930)

A thesis submitted in partial fulfillment of the requirements for the degree of
Master of Science in Quantitative Finance and Actuarial Sciences

Tilburg School of Economics and Management
Tilburg University

Supervised by:
Bertrand Melenberg

Second reader:
Anja De Waegenaere

Date: February 18, 2024

Abstract

The Covid-19 pandemic presented challenges for insurers and pension funds in valuing their liabilities due to excess mortality. Existing mortality models do not take into account these mortality shocks. This thesis aims to incorporate mortality shocks into a multi-population mortality model. This is achieved using data on deaths and exposures, obtained from the HMD and the Eurostat database, on a calibration period from 1900-2021. To capture mortality shocks in the model, the Li-Lee model is extended with a jump component in the time-series for the overall mortality trend. The newly developed model yields lower period and cohort life expectancies compared to the model developed by the The Royal Dutch Actuarial Association. Kannisto's closure method is applied to produce life expectancies for ages above 90. A sensitivity analysis explores the impact of using a shorter calibration period, excluding old mortality shocks. This analysis resulted in higher forecasted life expectancies and a narrower confidence interval for these forecasts compared to the original model.

Contents

1	Introduction	2
2	Literature review	5
2.1	Lee-Carter Model	5
2.2	Li-Lee Model	5
2.3	Models incorporating mortality shocks	6
2.4	The AG2022 Model	6
3	Data	8
4	Methods	14
4.1	Lee-Carter Model	15
4.2	Li-Lee Model	16
4.3	AG2022 Model	17
4.3.1	Kannisto	18
4.4	Incorporating mortality shocks into a multi-population mortality model	19
4.4.1	Parameter Calibration	19
4.4.2	Time Dynamics	20
4.4.3	Closure method of Kannisto	24
5	Results	25
5.1	Benchmark model	25
5.1.1	Parameter estimation	25
5.1.2	Outlier analysis	27
5.1.3	Forecasted mortality scenarios	29
5.2	Sensitivity analysis	37
5.2.1	Parameter estimation	37
5.2.2	Forecasted mortality scenarios	39
6	Conclusion	46
7	Recommendations	48
A	Appendix	51

1 Introduction

Since the second half of the 20th century, worldwide life expectancy has seen an increasing trend. Due to for example medical advances, better nutrition and increasing well-being in societies worldwide mortality rates constantly declined. In the Netherlands for example, the period life expectancy for a new born female increased from 72.6 years in 1950 to 83.1 years in 2020 (Statistics Netherlands, 2023). Of course, declining mortality rates are a good development for the human race. However, this improvement in period life expectancy challenges demographers, actuaries and life insurers. Uncertainty about future mortality rates raises risks about the estimation of future life expectancy. This risk for example appears for annuity providers, whose liabilities are linked to mortality developments. Lee and Carter (1992) were one of the first to describe mortality rates through dynamic time-series. Their model describes the evolution of the logarithm of the central death rate. The logarithm of the central death rate is decomposed in parameters which model the overall mortality trend, period effects, and age effects. Period effects are changes, through external factors, that occur at a specific time point and affect all age groups in a population simultaneously. Period calculations do not take into account future developments of death probabilities. Cohort effects, on the other hand, are effects of external factors that are specific to a particular cohort/generation of people. Cohort calculations take into account the trend of death probabilities. One drawback of the Lee and Carter model is that the model does not take into account cohort effects. To optimize the Lee Carter model, many researchers proposed extensions and alterations to the benchmark Lee Carter model. For example, Renshaw and Haberman (2006) proposed an extension to account for cohort effects. An other example of an extension of the Lee Carter model is that by Li and Lee (2005). Li and Lee extend the model by adding a term which accounts for a multi-population model. The model uses data from multiple countries, instead of one. This avoids diverging mortality forecasts for a specific group. Using data from multiple countries also enables the model to detect patterns in comparable countries or populations.

The Royal Dutch Actuarial Association (Koninklijk Actuarieel Genootschap), also abbreviated to AG, is an actuarial association in the Netherlands. The AG produces forecasts for death probabilities on bi-yearly basis. AG2022 is the most recent forecast table about the evolution of survival probabilities and life expectation in the Netherlands. To model these numbers, the AG makes use of the Li-Lee model mentioned earlier. The countries observed in this

multi-population model by the AG are European countries with similar GDP as the Netherlands.

Of course, mortality modeling is accompanied by risks, which are mitigated as well as possible. Mitigating all risks of a mortality model is not possible. Exceptional events could happen, leading to significant changes in mortality forecasts. The Covid-19 pandemic is an evident example of such an exceptional event. The Coronavirus took the lives of millions of people globally, leading to sudden mortality shocks in populations around the world. According to Statistics Netherlands, the increasing period life expectancy trend suddenly dropped from 80.5 years in 2019 to 79.7 in 2020 for new born males in the Netherlands. (Statistics Netherlands, 2023). Due to mortality shocks, forecasted death probabilities might become incorrect. This raises problems for actuaries and life insurers, since the calculations on their liabilities will be inaccurate. Actuaries worldwide are wondering how to incorporate the Covid-19 mortality shocks in their models. The AG makes use of an extended Li-Lee model, in which they add an extra component to account for the Covid-19 mortality shock (AG, 2022). The Continuous Mortality Investigations (CMI) also do research on mortality in the UK. In their mortality model it is decided to put a weight of 0% on the mortality data in 2020 and 2021, and a weight of 25% on the mortality data of 2022. All other years get a weight of 100 % (CMI, 2023).

The Lee Carter mortality model and its extensions mentioned earlier, do not take into account mortality shocks like Covid-19. In their paper, Lee and Carter (1992) used outlier detection methods to remove any influence of the mortality shock from the influenza pandemic in 1918 from their model. Because the Covid-19 pandemic has proven that mortality shocks are still occurring, and perhaps will occur in the future, mortality models should incorporate sudden mortality shocks. Existing literature about incorporating mortality shocks suggest several solutions to this topic including regime switching (Milonis et al., 2011), using extreme value theory (Chen and Cummins, 2010), or adding jump processes to the model ((Cox et al., 2006), (Chen and Cox, 2009)). Chapter 2 will provide a more in-depth discussion of the existing literature. Most of the models which include mortality shocks, extend the benchmark Lee-Carter model. However, as discussed above, the Lee Carter Model has some drawbacks. To produce a mortality model which includes shocks, a different approach is suggested. This thesis therefore focuses on the existing Li-Lee model used by the AG, and extends it by adding a jump process in line with Chen and Cox (2009) to account for mortality shocks and the drop in period life expectation. Data on deaths and exposures of European countries with similar GDP as the Netherlands is used in the estimation of the force of mortality, similar to the AG models. This estimation is done using likelihood maximization functions on the calibration period 1900-2021. An outlier analysis identifies spikes in the mortality trend during the world wars and during the Covid-19 pandemic. Because of such spikes, the time-series for the mortality trend is extended with a jump component. Afterwards, death probabilities and future period and cohort expectancies are estimated. Kannisto's closure

method (Kannisto, 1992) is used to obtain numbers on death probabilities for ages above 90, as data for high ages is scarce. The obtained estimates for future life expectancies are lower than the estimates by the AG. A sensitivity analysis is conducted to assess the impact of a shorter calibration period of 1970-2021. The new results on period and cohort life expectancy forecasts are slightly higher than before. Also, the confidence intervals for the period and cohort life expectancies are narrower compared to the same model with longer calibration period. Future research could build upon what the ideal calibration period should be. Furthermore, future research could incorporate jump events in the model differently, for example by using extreme value theory or regime switching models.

The next chapter provides an in-depth discussion of the existing literature. In Chapter 3 the data used in the model will be described. Chapter 4 elaborates on the methodology of the model and its calibration and estimation. In Chapter 5 the results of the model will be presented and a sensitivity analysis is conducted. Chapter 6 will have the concluding remarks and Chapter 7 will give recommendations for further research on this topic.

2 Literature review

As discussed in the introduction, the Lee-Carter model marked an important milestone in the field of mortality modeling. Lee and Carter (1992) laid the foundation for later advancements in mortality modeling. This chapter reviews the literature on the well known Lee Carter Model and its extensions. Particularly, the extension by Li-Lee and other extensions which focus on incorporating mortality shocks into their model.

2.1 Lee-Carter Model

In 1992, Lee and Carter came up with a model in their paper "Modeling and Forecasting U.S. Mortality" (Lee and Carter, 1992). Lee and Carter model the logarithm of the central death rate using a set of parameters. These parameters represent the overall mortality rate, period effects, and age effects, and can be estimated in an iterative manner using Singular Value Decomposition. Once the parameters are estimated, the future mortality rates can be forecasted using a random walk with drift. With these forecasted mortality rates, life expectancy can be calculated. The Lee-Carter model is elaborated more extensively in Chapter 4.

2.2 Li-Lee Model

Li and Lee (2005) consider an extension of the original Lee Carter model. Li and Lee found that the Lee Carter model caused problems when modeling two genders separately. To avoid diverging mortality forecasts for a specific gender, country, or population, Li and Lee consider an extended model. They model a country or a population as a part of a group, instead of modeling single countries or populations. To form these groups, countries or populations with for example similar socio-economic properties should be considered. Then, to the original Lee Carter model a set of parameters which account for random fluctuations and for the long-term trend of the whole group is added. In fact, the Li-Lee model can be seen as the sum of two Lee-Carter models. Also the Li-Lee model will be treated more extensively in Chapter 4.

2.3 Models incorporating mortality shocks

Both Lee and Carter (1992) and Li and Lee (2005) do not take mortality shocks like Covid-19 into consideration. As mentioned earlier, Lee and Carter used outlier detection to get rid of the effect on mortality caused by Influenza in 1918. Li and Lee disregarded the problem of mortality shocks as well. On the other hand, several other papers in the literature expand upon the original Lee Carter model by incorporating mortality shocks into the model.

Milidonis et al. (2011) extend the Lee Carter model by adding a Markov regime switching model. When a mortality shock occurs, the model switches to a high-volatility regime for as long as the duration of the mortality shock. The different regime states are added into the time series model. Using maximum likelihood estimation, the transition probabilities between the regime states are estimated.

Using Extreme Value Theory, Chen and Cummins (2010) try to enhance the Lee Carter model. First, the same steps as the Lee Carter model are followed. To model small variations in the mortality parameter, a random walk with drift is considered, just like in the Lee Carter model. To this, Chen and Cummins (2010) add a variable for the mortality improvement. Then the Peaks-over-Threshold, a method for modeling extreme values, is used. A threshold is chosen from which onward events are considered extreme. In this way the model provides a good fit for the central regions and for the tail of the mortality improvement distribution simultaneously.

Cox et al. (2006) propose a jump process to include mortality shocks into the Lee Carter model. The proposed jump process adds a permanent jump effect to the random walk with drift. But, since most mortality shocks like the 1918 influenza pandemic, or the 2004 tsunami do not have permanent shocks, Chen and Cox (2009) proposed an updated model to add transitory jumps instead of permanent jumps. The mortality numbers from the Covid-19 pandemic indicate a rise in mortality rates during its peak, followed by a return to normal rates once the pandemic is brought under control. Therefore, a transitory jump effect should be more appropriate for the Covid-19 pandemic as well.

2.4 The AG2022 Model

The Royal Dutch Actuarial Association (AG) uses its own model for forecasting survival probabilities of the Dutch population. The model behind the most recent forecast table, AG2022, has a few adaptations from earlier models used by the AG. To estimate mortality rates and project them into the future, the AG makes use of the Li-Lee model as a basis (AG, 2022). For data until 2020 (pre-Covid), the standard Li-Lee model is used. In the introduction it is mentioned that the Dutch population is considered as part of a group of populations. This group consists of Austria, Belgium, Denmark, Germany, Finland, France, Iceland, Ireland, Luxembourg, the Netherlands, Norway, United Kingdom, Sweden and Switzerland. These countries have in common that the value of their Gross Domestic Product (GDP) is above the European average and

that the countries are located in North- and West-Europe. GDP is used as a measure because wealth has a positive correlation with life expectancy. In this way the AG may possibly find any common patterns in a larger group of populations. To incorporate the excess mortality due to Covid-19 into the model, the AG makes use of an extension inspired by the Lee-Carter model. To the Li-Lee model a component is added which models the mortality deviation from 2020 onward. This component is only added for ages above 55, since Covid-19 had negligible impact on mortality rates for ages below 55. The extension due to Covid-19 is a transitory one, since the added component has a half-life duration of one year, so the effect of Covid-19 is slowly disappearing in the model.

3 Data

Mortality models are essential due to the fact that mortality levels continuously are changing over the years. Mortality rates are in a declining trend, and therefore the (period) life expectancy is in an upward trend as depicted in Figure 3.1 (HMD, 2023). Consequently, modeling mortality becomes crucial to provide insurers and pension funds with accurate data and forecasts, enabling them to assess and value their liabilities effectively.

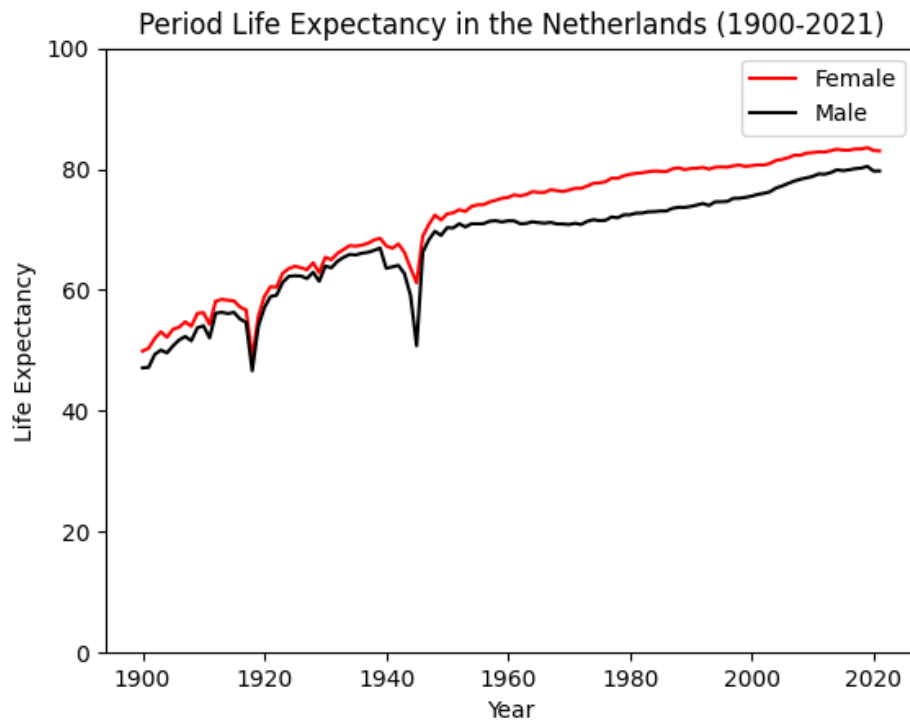


Figure 3.1: The evolution of period life expectancy in the Netherlands for females and males in 1900-2021. Source: HMD (2023)

The increasing period life expectancy in the Netherlands from 1900 onward exhibits a few downward spikes, these spikes represent mortality shocks. Specifically, these shocks are the Influenza pandemic in 1918, the second world war in 1940-1945 (especially for males), strengthened by the Dutch famine of 1944-1945, and of course the Covid-19 Pandemic in 2020 and 2021. Such shocks, like the one observed due to the Covid-19 pandemic (see Figure 3.2), underscore the importance of incorporating these shocks into a mortality model.

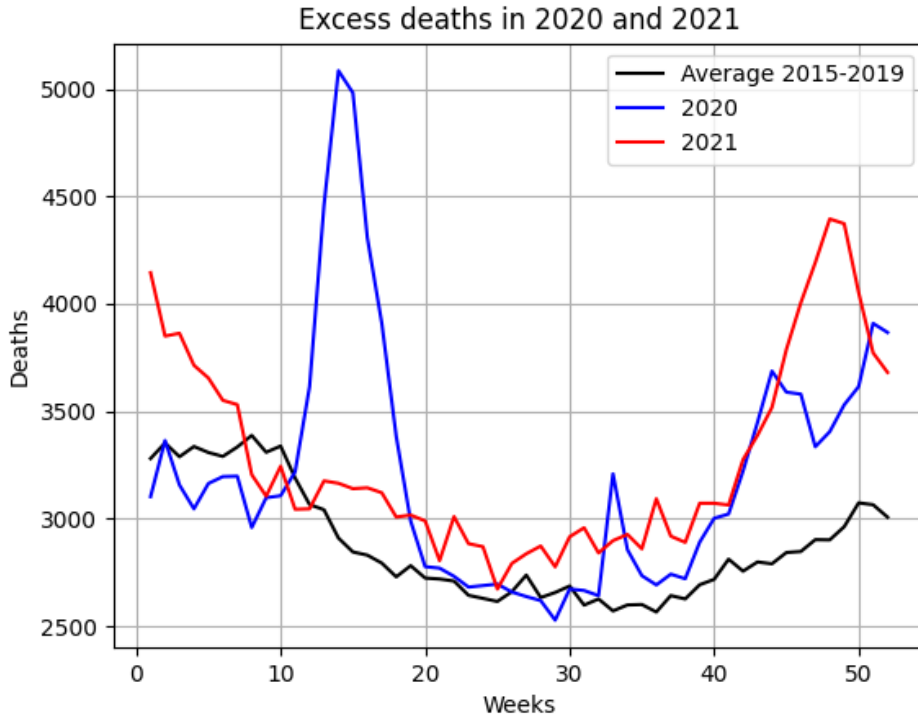


Figure 3.2: Excess deaths in the Netherlands during the Covid-19 pandemic. The graphs represent the number of deaths per week in 2020 and 2021 compared to the average deaths per week in 2015-2019. Source: STMF (2023)

As previously mentioned in the introduction and in Chapter 2, the model considered in this thesis builds upon the Li-Lee Model. In this model, data for multiple countries with similar socio-economic properties is considered, in this case, similar GDP is considered. I choose to use the same countries as the AG uses for their mortality model, excluding the UK. The new multi-population model therefore considers data during the time period 1900-2021 from Austria, Belgium, Denmark, Finland, France, Germany, Iceland, Ireland, Luxembourg, Norway, The Netherlands, Sweden and Switzerland. The data that is used in the model are the observed deaths and exposures from these countries. Unfortunately, from the countries Germany¹, Austria, Ireland and Luxembourg limited data between 1900 and 1960 is observable. Data from these countries are consecutively added whenever the data becomes available. Also, for the Belgium data there is a gap in the data from 1914 to 1918. Figure 3.3 depicts the countries in the data-set and the starting year of the data availability.

¹Until 1990 East-Germany and West-Germany were distinct countries. The number of deaths and the exposure from only West-Germany were used before 1990. From 1990 onwards, the number of deaths and exposures of East-Germany and West-Germany are aggregated

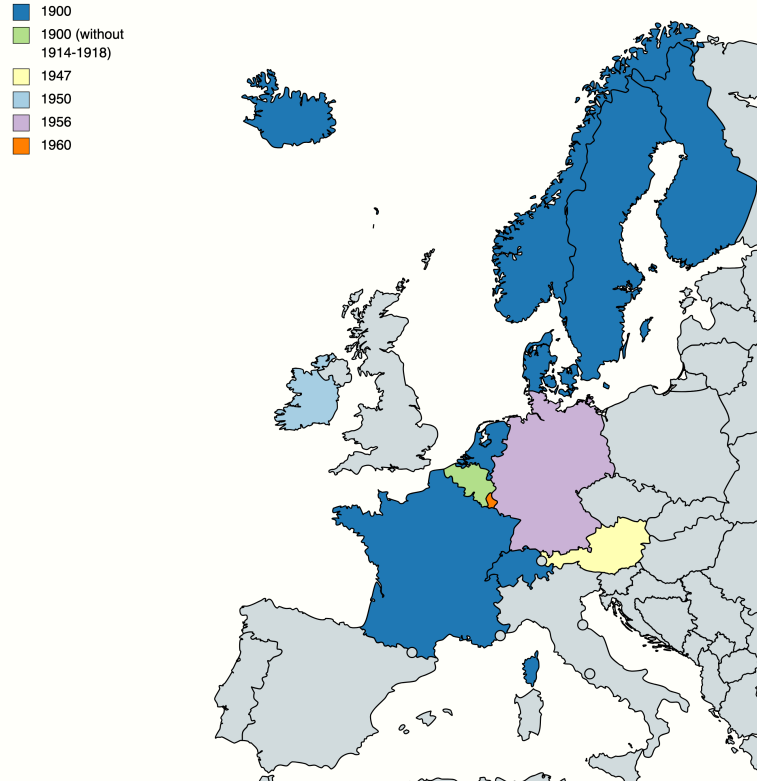


Figure 3.3: Visualization of the European countries used in the data-set for this thesis. The colors indicate the starting year of the data availability

As a benchmark I choose to define the set of all countries depicted in Figure 3.3 calibrated over the period $\mathcal{T} = \{1900, \dots, 2021\}$. A sensitivity analysis will be conducted in Chapter 5 to assess whether a shorter calibration period, $\tilde{\mathcal{T}} = \{1970, \dots, 2021\}$, has a major influence on the results.

It is important to note that, beyond the Netherlands, the other countries experienced excess mortality as well due to the Covid-19 pandemic. See Figure 3.4 to visualize the excess mortality for some of these countries (HMD, 2023). Similar graphs for the remaining countries can be found in Appendix A. In addition, these countries follow roughly similar trends of life expectancy as observed in Figure 3.1 in The Netherlands. See Figure 3.5 to visualize the trends in period life expectancy for some of the countries in the data-set. Again, Appendix A contains similar graphs for the remaining countries in the data-set.

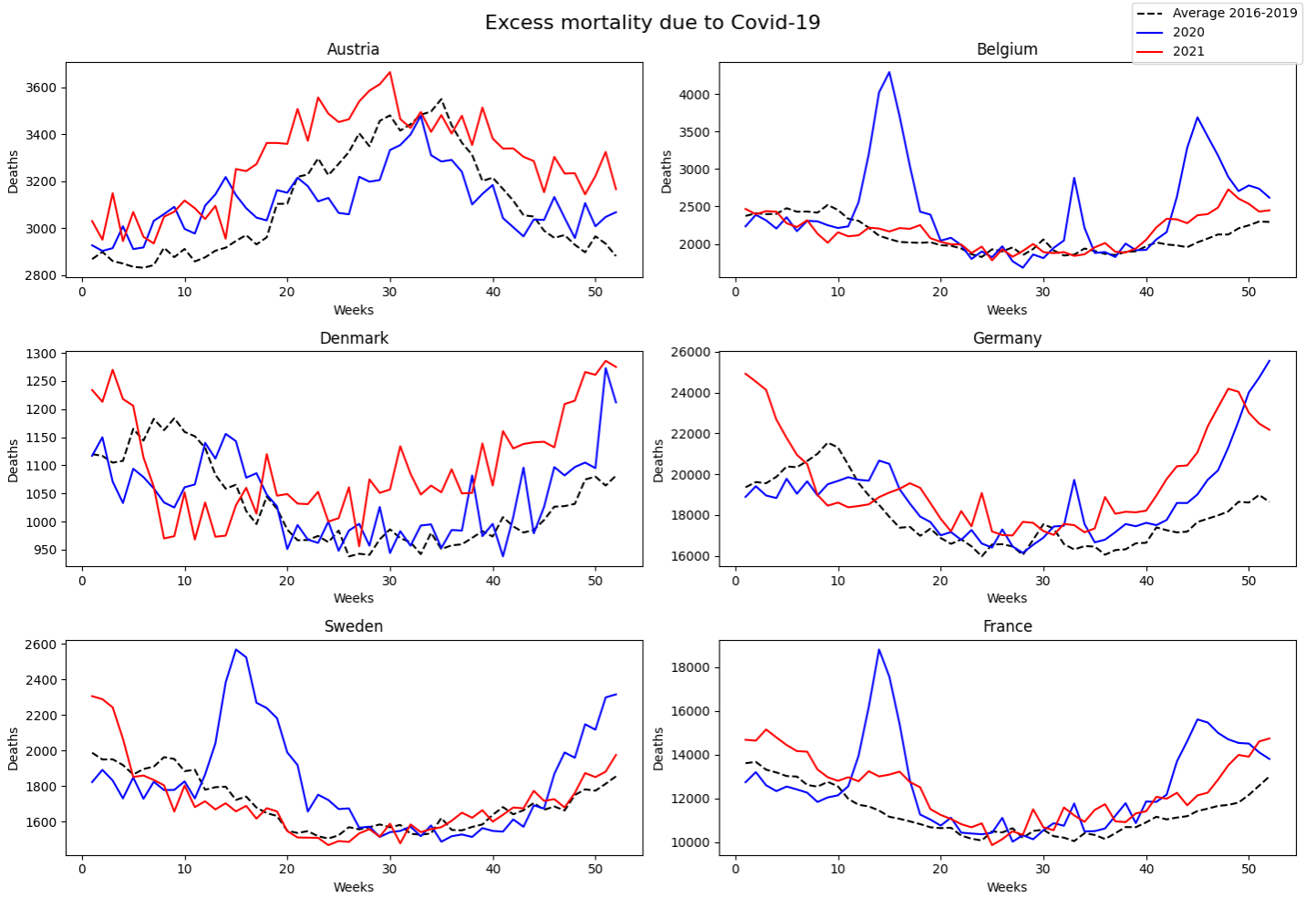


Figure 3.4: Excess deaths in Austria, Belgium, Denmark, Germany, Sweden, and France during the Covid-19 pandemic. The graphs represent the number of deaths per week in 2020 and 2021 compared to the average deaths per week in 2016-2019. Source: STMF (2023)

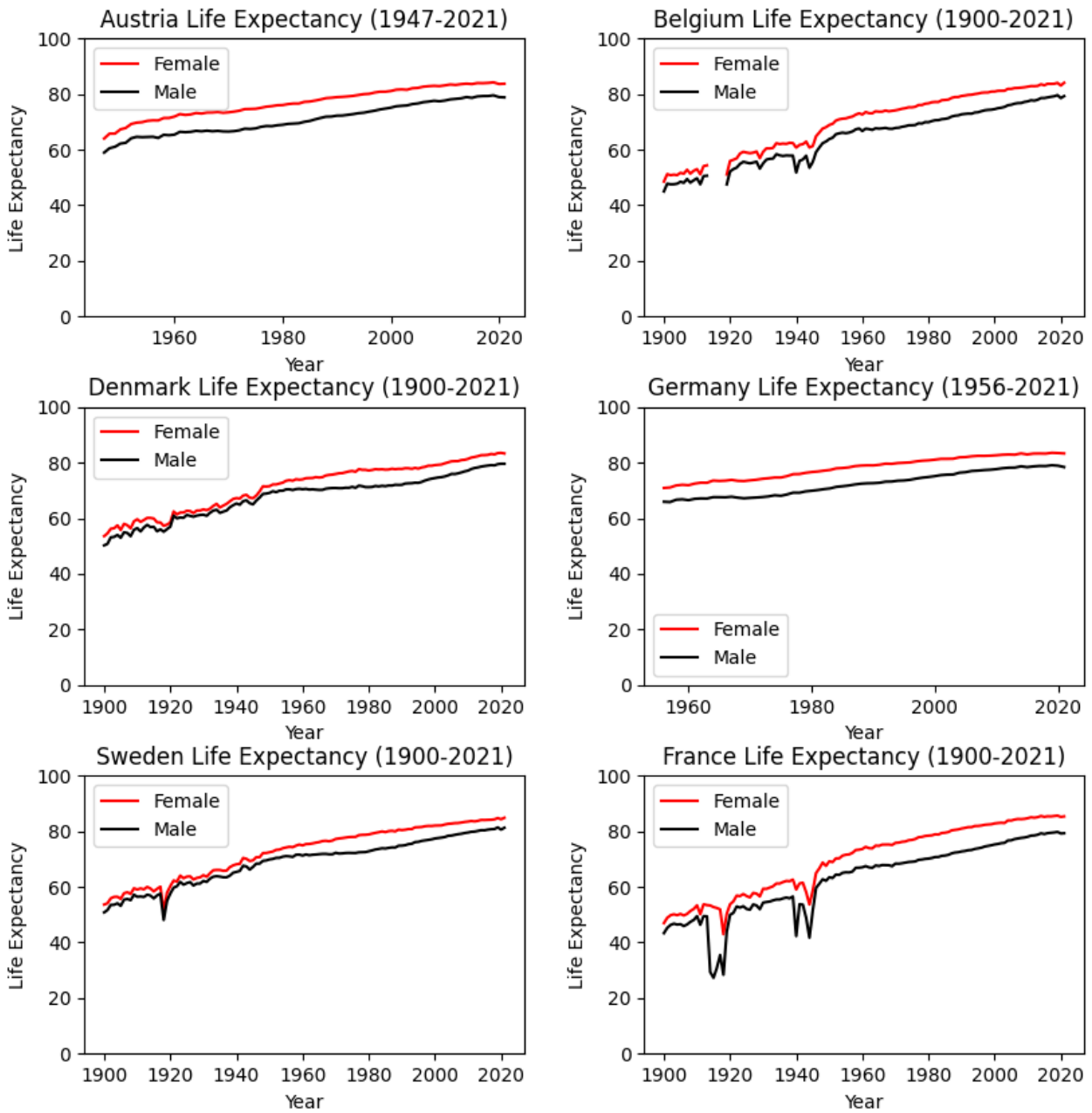


Figure 3.5: The evolution of male and female period life expectancy in Austria, Belgium, Denmark, Germany, Sweden, and France for different time periods. Source: HMD (2023)

To create estimates and forecasts for the model, data on deaths and exposures are required. For every country (i), age (x) and year (t), deaths and exposures from the data are denoted by $D_{x,t}^i$ and $E_{x,t}^i$ respectively. Here, $i \in \mathcal{I} = \{Austria, Belgium, Denmark, Germany, Finland, France, Iceland, Ireland, Luxembourg, Norway, the Netherlands, Sweden, Switzerland\}$, $x \in \mathcal{X} = \{0, \dots, 90\}$, and $t \in \mathcal{T} = \{1900, \dots, 2021\}$

The data set is obtained from the Human Mortality Database (HMD), and supplemented with data from the Eurostat database (EUROS, 2023) for the years and countries where information is not available in the HMD. Appendix A provides a table for the data sources. It is verified that the definitions and data from the Eurostat database align with the definitions and data from the HMD, as the data for overlapping years is identical.

The data only includes ages up to 90 due to the lack of data for ages above 90. Mortality rates for higher ages are modeled using a technique introduced by Kannisto (1992). A more detailed explanation of Kannisto's closure method will be provided in Chapter 4.

Fortunately, data on deaths is directly observable in both the HMD and Eurostat database. However, data on exposures in period format is not observed in the Eurostat database. To find the (period) exposures, first two other quantities are needed:

- $P_{x,t}^i$: The population on January 1st with age between x and $x + 1$ in year t . This is simply the population size.
- $C_{x,t}^i$: The number of deaths in year t , who would have been between x and $x + 1$ years old on December 31st in year t . This is the cohort number of deaths.

To convert these quantities into the exposures in period format, which are required for the model, the Methods Protocol established by the HMD's is consulted (Wilmoth et al., 2007).

For $x > 0$:

$$E_{x,t}^i = \frac{1}{2} \left(P_{x,t}^i + P_{x,t+1}^i \right) + \frac{1}{6} \left(\frac{1}{2} C_{x,t}^i - \frac{1}{2} C_{x+1,t}^i \right), \quad (3.1)$$

and for $x = 0$:

$$E_{0,t}^i = \frac{1}{2} \left(P_{0,t}^i + P_{0,t+1}^i \right) + \frac{1}{6} \left(C_{0,t}^i - \frac{1}{2} C_{1,t}^i \right). \quad (3.2)$$

4 Methods

In this chapter, the Lee-Carter model, the Li-Lee model, and the AG2022 model are discussed in more detail and a new model, incorporating mortality shocks, is introduced. The Li-Lee model is an extension of the Lee-Carter model, and the newly introduced model is built upon the framework established by the Li-Lee model. The goal of this thesis is to propose a model which takes into account mortality shocks and can be used to model and forecast mortality in times of a pandemic. For this, a mathematical model is necessary which provides death probabilities.

The main interest is $m_{x,t}^i$, the central death rate, and is defined as

$$m_{x,t}^i = \frac{D_{x,t}^i}{E_{x,t}^i}, \quad (4.1)$$

where $D_{x,t}^i$ is the number of deaths in population i , for age x , at time t and $E_{x,t}^i$ is the exposure in population i , for age x , at time t , and is thoroughly discussed in Chapter 3.

If it is assumed that the force of mortality ($\mu_{x,t}^i$) is constant during a certain year for a certain age, it can be concluded that the central death rate is equal to the force of mortality.

$$\mu_{x+\zeta_1, t+\zeta_2}^i = \mu_{x,t}^i \quad \forall i \in \mathcal{I}, x \in \mathcal{X}, t \in \mathcal{T}, \text{ and } \zeta_1, \zeta_2 \in [0, 1). \quad (4.2)$$

i.e. if (4.2) holds, then the MLE estimate of $\mu_{x,t}^i$, yields that $\hat{\mu}_{x,t}^i = m_{x,t}^i$ (Melenberg, 2021). Assuming this, the death probabilities can be calculated by:

$$q_{x,t}^i = 1 - e^{-m_{x,t}^i}. \quad (4.3)$$

Future deaths and exposures are, of course, not observable, and therefore the future central death rate is also not observable. These numbers need to be modeled. The Lee-Carter model and the Li-Lee model, model the central death rate directly. With these modeled central death rates, one can produce for example a forecast table for life expectations, just like the AG does bi-yearly.

4.1 Lee-Carter Model

As discussed in Chapter 2, Lee and Carter (1992) proposed a model to forecast U.S. mortality rates. Lee and Carter model the logarithm of the central death rate as follows:

$$\log(m_{x,t}) = \alpha_x + \beta_x \kappa_t + \epsilon_{x,t}. \quad (4.4)$$

Note, that in the Lee-Carter model, the superscript i for the population is omitted. This omission occurs because the Lee-Carter model only makes estimates for one population. α_x is an age-dependent constant that represents the evolution of the mortality trend. κ_t is a time-varying mortality index, and β_x denotes the age specific sensitivity to changes in κ_t . $\epsilon_{x,t}$ represents the error term and it is assumed that it has zero mean and satisfies homoskedasticity. The model clearly is overparameterized, hence it is necessary to impose some normality constraints for identification. Lee and Carter propose:

$$\sum_{x \in \mathcal{X}} \beta_x = 1 \text{ and } \sum_{t \in \mathcal{T}} \kappa_t = 0. \quad (4.5)$$

With these constraints, the estimate of α_x becomes the average of the logarithm of the central death rate over time:

$$\hat{\alpha}_x = \frac{1}{T} \sum_{t=1}^T \log(m_{x,t}). \quad (4.6)$$

Here, T represents the length of the calibration period.

To solve the model, Lee and Carter suggest a two-step procedure. Since ordinary regression methods are not applicable, Lee and Carter make use of Singular Value Decomposition (SVD) on the matrix of $\log(m_{x,t}) - \hat{\alpha}_x$ in the first step. The estimates of β_x and κ_t are obtained in this way. In the second step, the estimates of α_x and β_x from the first step are used to obtain new estimates for κ_t . This is done iteratively such that the implied number of deaths are equal to the observed number of deaths.

$$D_t = \sum_{x \in \mathcal{X}} (N_{x,t} e^{\alpha_x + \beta_x \kappa_t}). \quad (4.7)$$

Here, $D_t = \sum_x D_{x,t}$ are the observed number of deaths at time t for all ages, and $N_{x,t}$ is the population of age x at time t .

After fitting the model, mortality projections are obtained using auto-regressive integrated moving average (ARIMA(p,d,q)) time series on κ_t . Lee and Carter use a random walk with drift to model the evolution of κ_t . This is also known as an ARIMA(0,1,0) model:

$$\kappa_t = \mu + \kappa_{t-1} + \xi_t, \quad (4.8)$$

where μ is the drift term, and ξ_t is the error term with mean 0 and variance σ_ξ^2 . It is assumed that the error term ξ_t is not correlated and is independent of $\epsilon_{x,t}$ from (4.4). Given this procedure, mortality projections can be easily derived using extrapolation.

To account for the Influenza mortality shock in 1918, Lee and Carter propose an intervention model when estimating the evolution of κ_t :

$$\kappa_t = \mu + \kappa_{t-1} + \theta \cdot flu + \xi_t. \quad (4.9)$$

Here, flu is a dummy variable for the year 1918, and θ is the coefficient on the dummy variable which captures the magnitude of the change in κ_t in 1918.

4.2 Li-Lee Model

Li and Lee (2005) found that the original Lee-Carter model leads to diverging mortality forecasts. When using the original Lee-Carter model for males and females separately, they found that the β_x in (4.4) and the μ in (4.8) had significant differences. This would lead to very different mortality forecasts in the long run for males and females in a specific country. The same divergence problem occurs when forecasting mortality rates in different provinces of a country separately. To avoid the problem of diverging mortality forecasts, Li and Lee suggest that all populations or members of a group should have the same β_x and the same drift term (μ) for κ_t . It is then a sufficient condition that all populations or members of a group share the same values for β_x and κ_t , denoted by B_x and K_t .

Their multi-populations model for modeling and forecasting mortality is as follows:

$$\log(m_{x,t}^i) = \alpha_x^i + B_x K_t + \beta_x^i \kappa_t^i + \epsilon_{x,t}^i. \quad (4.10)$$

The normalizations to make the model identifiable are:

$$\sum_{x \in \mathcal{X}} B_x = 1, \quad \sum_{t \in \mathcal{T}} K_t = 0, \quad \sum_{x \in \mathcal{X}} \beta_x = 1 \text{ and } \sum_{t \in \mathcal{T}} \kappa_t = 0. \quad (4.11)$$

The parameters B_x and K_t are estimated for the whole group in the same way as in the original Lee-Carter Model from Chapter 4.1. The K_t is then re-estimated to fit the average life expectancy of the group. $B_x K_t$ is the common factor for every population i in the group. Also in this case, to model the evolution of K_t , a random walk with drift is used to forecast the common trend of the group's future mortality, similar to (4.8):

$$K_t = \mu + K_{t-1} + \xi_t. \quad (4.12)$$

α_x^i is an age-dependent constant that captures the general evolution of the mortality trend for population i . Considering the constraints of (4.11), the estimate of α_x^i now again becomes the average of the logarithm of the central death rate over time for population i . This is a similar derivation as (4.6)

$$\hat{\alpha}_x^i = \frac{1}{T} \sum_{t=1}^T \log(m_{x,t}^i). \quad (4.13)$$

$(\alpha_x^i + B_x K_t)$ is called the common factor model for population i . Next, SVD is

applied to the residual matrix of the common factor model $\log(m_{x,t}^i) - \alpha_x^i - B_x K_t$ to obtain estimates for β_x^i and κ_t^i . κ_t^i is the population specific time-varying mortality index and β_x^i is the age specific sensitivity to changes in κ_t^i . $\beta_x^i \kappa_t^i$ captures the deviation of population i 's mortality rate variation from to the common factor's mortality rate variation.

To obtain mortality projections, Li and Lee propose a first-order autoregressive model (AR(1)) for the evolution of κ_t^i :

$$\kappa_t^i = c_0^i + c_1^i \kappa_{t-1}^i + \sigma^i \delta_t^i, \quad \delta_t^i \sim N(0, 1). \quad (4.14)$$

Here, c_0^i and c_1^i are the coefficients and σ^i is the standard deviation of the first-order autoregressive model.

4.3 AG2022 Model

The AG makes use of a model based on the Li-Lee model, which is extended with a factor to add the effect on mortality due to Covid-19 (AG, 2022).

$$\log(m_{x,t}^i) = \log(m_{x,t}^{i,pre-cov}) + \log(o_{x,t}^i). \quad (4.15)$$

Here, $\log(m_{x,t}^{i,pre-cov})$ is the part of the model based on the Li-Lee model, not incorporating the mortality shock due to Covid-19. It is modeled as:

$$\log(m_{x,t}^{i,pre-cov}) = A_x + B_x K_t + \alpha_x^i + \beta_x^i \kappa_t^i, \quad (4.16)$$

where A_x , B_x and K_t are the parameters for the total group of countries (Austria, Belgium, Denmark, Germany, Finland, France, Iceland, Ireland, Luxembourg, Norway, the Netherlands, United Kingdom, Sweden and Switzerland) and α_x^i , β_x^i and κ_t^i are the parameters for the Dutch population. The parameters of the Dutch population are modeled as the deviation of the Dutch population compared to the whole group of populations. The parameters are based on the quotient of these two factors. The time-series dynamics consist of a random walk with drift for the total group and a first-order autoregressive model for the Dutch deviation, similar to the Li-Lee model:

$$K_t = \mu + K_{t-1} + \xi_t \quad (4.17)$$

$$\kappa_t^i = c_0^i + c_1^i \kappa_{t-1}^i + \delta_t^i. \quad (4.18)$$

To add the effect of the Covid-19 mortality shock, the AG extended their model by the factor $\log(o_{x,t}^i)$ from (4.15). The model behind this factor is inspired by the Lee Carter model and uses weekly data from 2020 and 2021 to estimate the model. $\log(o_{x,t}^i)$ is fading out slowly in future years, as it has a half-life duration of one year.

4.3.1 Kannisto

As mentioned in the previous chapter, the AG makes mortality estimates for the the age class 91-120 using a method developed by Kannisto (1992). Due to a lack of data for that specific age group, the AG decided to make use of this extrapolation technique. In the AG2022 model the Kannisto method applied is slightly different from the previous models developed by the AG.

First, the parameters A_x , B_x , α_x^i , and β_x^i are estimated for ages 0 to 90 using the methods described earlier in this chapter. Afterwards, the parameters A_x , B_x , α_x^i , and β_x^i for ages 91-120 are determined using extrapolation techniques based on a logistic regression developed by Kannisto (1992).

In previous AG models, for example the AG2020 model, not the parameters, but the estimates of the force of mortality, $\mu_{x,t}^i$, are extrapolated (AG, 2020). The force of mortality for ages 80 up to 90, for a specific population i , at a certain time t , are extrapolated using a logistic regression. In this way estimates are obtained for the force of mortality for ages 91 to 120 for that specific population i at time t .

4.4 Incorporating mortality shocks into a multi-population mortality model

In this section, the new model will be introduced. A multi-population mortality model with jumps to account for mortality shocks is modeled. Simply performing outlier analysis and consequently remove the effect of a mortality shock should not be the solution. As Chen and Cox (2009) point out, outliers should not be neglected, because for example mortality securitization and pricing catastrophe risks depends on these outliers. Furthermore, for calculating solvency capital requirements these outliers are of great importance as well. The model can be seen as an extension of the Li-Lee model, inspired by the extension of the Lee-Carter model by Chen and Cox (2009). Since historical mortality shocks like the 1918 influenza pandemic or the 2004 earthquake and tsunami in the Indian Ocean, did not have a permanent effect on mortality rates, a transitory effect is added to the model. This ensures that the effects of a mortality shock are disappearing over time and will not effect the mortality rates permanently.

The basis of the model is similar to the AG models before Covid-19. The logarithm of the force of mortality is modeled as:

$$\log(\mu_{x,t}^{g,i}) = A_x^g + B_x^g K_t^g + \alpha_x^{g,i} + \beta_x^{g,i} \kappa_t^{g,i}. \quad (4.19)$$

Here, the newly introduced parameter $g \in \mathcal{G} = \{\text{Male, Female}\}$ specifies the gender. Again, A_x^g , B_x^g and K_t^g are the parameters for the reference group of European countries $\mathcal{I} = \{\text{Austria, Belgium, Denmark, Germany, Finland, France, Iceland, Ireland, Luxembourg, Norway, The Netherlands, Sweden, Switzerland}\}$, for age x at time t .

$\alpha_x^{g,i}$, $\beta_x^{g,i}$ and $\kappa_t^{g,i}$ are the parameters for a specific population, in this case that is the Dutch population, from now on denoted by $\alpha_x^{g,NL}$, $\beta_x^{g,NL}$ and $\kappa_t^{g,NL}$.

4.4.1 Parameter Calibration

Contrary to the SVD method which is used by Lee and Carter and by Li and Lee to estimate the parameters, an other approach is selected. Following the approach by Brouhns et al. (2002), parameters of the model are calibrated using a Poisson likelihood function. The calibration is done for both males and females separately. For notational convenience, the superscript g is left out in the following steps.

First, the parameters for the total European reference group are calibrated. The estimates of the parameters A_x , B_x , and K_t are determined using a Poisson likelihood function. This is possible because of the assumption that the total deaths in the European reference group, $D_{x,t}^{EU}$, follows a Poisson distribution with mean $E_{x,t}^{EU} \mu_{x,t}^{EU}$ (Brouhns et al., 2002). Here, EU in the superscript underscores the fact that these are the parameters for the European reference group. $E_{x,t}^{EU}$ are the aggregated exposures in the European reference group for age x at time t , and $\mu_{x,t}^{EU} = e^{A_x + B_x + K_t}$ is the force of mortality for the European reference group for age x at time t . Therefore, instead of modeling

$m_{x,t}^g$ directly like in the Lee Carter model, $D_{x,t}^g | E_{x,t}^g \sim \text{Poisson}(E_{x,t}^{EU} \mu_{x,t}^{EU})$ is modeled.

In order to obtain a likelihood function, the exposures $E_{x,t}^{EU}$ and deaths $D_{x,t}^{EU}$ for all countries in \mathcal{I} , during $t \in \{1900, \dots, 2021\}$, for all ages $x \in \{0, \dots, 90\}$ are used. To obtain estimates for the parameters, the following Poisson likelihood function is maximized:

$$\max_{\{A_x, B_x, K_t\}} \prod_{x \in \{0, \dots, 90\}} \prod_{t \in \{1900, \dots, 2021\}} \frac{\left(E_{x,t}^{EU} \mu_{x,t}^{EU}\right)^{D_{x,t}^{EU}} \exp\left(-E_{x,t}^{EU} \mu_{x,t}^{EU}\right)}{D_{x,t}^{EU}!}. \quad (4.20)$$

To obtain a unique solution for the estimates of the parameters, the following constraints are imposed, with a small difference compared to (4.11) from the Li-Lee model.

$$\sum_{t \in \{1900, \dots, 2021\}} K_t = 0, \quad \text{and} \quad \sum_{x \in \{0, \dots, 90\}} B_x^2 = 1. \quad (4.21)$$

Once the estimates \hat{A}_x , \hat{B}_x , and \hat{K}_t are obtained, they will be used in the following step. The estimate for the central death rate of the European reference group is now equal to: $\hat{\mu}_{x,t}^{EU} = \exp(\hat{A}_x + \hat{B}_x \hat{K}_t)$

Next, the country specific parameters α_x^{NL} , β_x^{NL} and κ_t^{NL} are estimated using a Poisson likelihood maximization again. This time the exposures $E_{x,t}^{NL}$ and deaths $D_{x,t}^{NL}$ for the Netherlands for ages $x \in \{0, \dots, 90\}$ and time $t \in \{1900, \dots, 2021\}$ are used in the function. The following Poisson likelihood function is maximized:

$$\max_{\{\alpha_x, \beta_x, \kappa_t\}} \prod_{x \in \{0, \dots, 90\}} \prod_{t \in \{1900, \dots, 2021\}} \frac{\left(E_{x,t}^{NL} \mu_{x,t}^{NL}\right)^{D_{x,t}^{NL}} \exp\left(-E_{x,t}^{NL} \mu_{x,t}^{NL}\right)}{D_{x,t}^{NL}!}, \quad (4.22)$$

where, $\mu_{x,t}^{NL} = \hat{\mu}_{x,t}^{EU} \exp(\alpha_x^{NL} + \beta_x^{NL} \kappa_t^{NL}) = \exp(\hat{A}_x + \hat{B}_x \hat{K}_t) \exp(\alpha_x^{NL} + \beta_x^{NL} \kappa_t^{NL})$.

The estimates \hat{A}_x , \hat{B}_x , and \hat{K}_t were obtained in the previous step.

Also in this step, to avoid identification problems, the following normalization constraints are imposed, again with a small difference compared to the constraints in the Li-Lee model (4.11):

$$\sum_{t \in \{1900, \dots, 2021\}} \kappa_t = 0, \quad \text{and} \quad \sum_{x \in \{0, \dots, 90\}} \beta_x^2 = 1. \quad (4.23)$$

Through this approach, the estimates $\hat{\alpha}_x^{NL}$, $\hat{\beta}_x^{NL}$, and $\hat{\kappa}_t^{NL}$ are also derived.

4.4.2 Time Dynamics

The next step is to construct the time-series for the parameters K_t and κ_t^{NL} , and include a jump process to account for mortality shocks.

The difference with the usual Li-Lee model is the fact that a jump component is included in the time series for the mortality factor K_t . Just like in the Li-Lee model (4.12), a random walk with drift, also known as an ARIMA(0,1,0)

model, is used to model the evolution of K_t and to forecast the common trend of the reference group's future mortality. However, to this time-series a jump component is added to account for a mortality shock in the whole European group, in line with Chen and Cox (2009).

I choose to include the jump component for the whole European group instead of including the jump only for the Dutch deviation. In the winter of 1944-1945 the Dutch Famine resulted to excess deaths only in the Netherlands. For this reason, one could choose to only add a jump component for the Dutch deviation. However, due to the globalization of the world, the easy ways to travel across countries, and due to the fact that the Covid-19 pandemic affected the whole world, future mortality shocks will affect multiple countries simultaneously and will not be limited to impacting just a single country in my opinion. Before including jumps in the model, an outlier analysis is conducted to identify whether spikes exist in the mortality index K_t . Note, that this is the mortality index for the European reference group. After having obtained estimates for K_t , the yearly change in K_t is calculated. The Z-Score method is used to detect outliers within the differenced values for K_t . The Z-Score, which measures the number of standard deviations an observation is from the mean, is calculated for each year. A predefined threshold is chosen to determine which observations qualify as outliers. An outliers is defined as a data point from which the Z-Score exceeds the specified threshold. The next steps will elaborate on how to deal with these outliers by including a jump in the model.

First, the time series model for K_t without jump is introduced.

$$\tilde{K}_t = \mu + \tilde{K}_{t-1} + \sigma Q_t, \quad (4.24)$$

where μ is the constant drift term, σ is the constant error term, and Q_t is a standard normal variable.

Simply adding an extra term for a shock effect to (4.24) will cause the shock effect to endure forever in all future values of \tilde{K}_t . Since most causes of mortality shocks only have a temporary effect, effects of a jump in a previous time-period should be nullified.

Let N_t represent the indicator of whether a mortality shock occurred in year t . $N_t = 0$ in a year with no mortality shock, and $N_t = 1$ if a mortality shock occurred in year t . The probability of a shock is p , therefore:

$$N_t = \begin{cases} 1, & \text{with probability } p \\ 0, & \text{with probability } 1 - p. \end{cases} \quad (4.25)$$

The severity of the shock is measured by Y_t . It is assumed that Y_t is an identically independently normally distributed variable with mean m and standard deviation s . It is also assumed that at most one jump per year can occur. Note, that N_t and Y_t are assumed to be independent of Q_t .

The time series for K_t can now be modeled as an ARIMA(0,1,0) model, ex-

tended by the factor $N_t Y_t - N_{t-1} Y_{t-1}$:

$$\begin{aligned} K_t &= \tilde{K}_t + N_t Y_t - N_{t-1} Y_{t-1} \\ &= K_{t-1} + \mu + \sigma Q_t + N_t Y_t - N_{t-1} Y_{t-1}. \end{aligned} \quad (4.26)$$

Next, κ_t^{NL} follows the same time dynamics as in the original Li-Lee model. The process is a first-order autoregressive model with constant term, also known as an AR(1) model.

$$\kappa_t^{NL} = c_0 + c_1 \kappa_{t-1}^{NL} + \sigma_\delta \delta_t, \quad (4.27)$$

where c_0 and c_1 are parameters of the time series, σ_δ is the error term and δ_t is a standard normal variable.

Time-series parameter calibration

To predict future mortality rates and life expectancies, it is essential to project the time series of K_t and κ_t into the future. To achieve this, the parameters in (4.26) and (4.27) must be calibrated.

Let $z_t = K_t - K_{t-1}$. If K_t has T observations, then z_t will have $T - 1$ observations. z_t can be modeled as:

$$z_t = \mu + \sigma Q_t + N_t Y_t - N_{t-1} Y_{t-1}. \quad (4.28)$$

Maximum likelihood estimation is now utilized to calibrate the parameters. Lin and Cox (2008) used a continuous-time model to include transitory mortality shocks into their model. Following their argument that the likelihood of an extreme mortality event has a very low probability, it is assumed that the correlation between shocks is negligible, in other words, shocks are assumed to be independent of each other. Therefore, it is assumed that z_t is independent of all future z_t and basic maximum likelihood estimation can be performed.

The distribution of z_t depends on whether a jump occurs or not. A jump event can occur in year t , in year $t - 1$, in both years or in neither of these years. Conditioning on the occurrence of a jump event, the distribution can be described as follows:

Jump event	Mean	Variance	Probability
$N_t = 0, N_{t-1} = 0$	μ	σ^2	$(1-p)(1-p)$
$N_t = 1, N_{t-1} = 0$	$\mu + m$	$\sigma^2 + S^2$	$p(1-p)$
$N_t = 0, N_{t-1} = 1$	$\mu - m$	$\sigma^2 + S^2$	$(1-p)p$
$N_t = 1, N_{t-1} = 1$	μ	$\sigma^2 + 2S^2$	p^2

The probability density function of z_t , $f(z_t)$, is now equal to

$$\begin{aligned}
f(z_t) &= f(z_t|N_t = 0, N_{t-1} = 0)\Pr(N_t = 0, N_{t-1} = 0) \\
&+ f(z_t|N_t = 1, N_{t-1} = 0)\Pr(N_t = 1, N_{t-1} = 0) \\
&+ f(z_t|N_t = 0, N_{t-1} = 1)\Pr(N_t = 0, N_{t-1} = 1) \\
&+ f(z_t|N_t = 1, N_{t-1} = 1)\Pr(N_t = 1, N_{t-1} = 1) \\
&= \left(\frac{1}{\sigma\sqrt{2\pi}} e^{-\frac{1}{2}\left(\frac{z_t-\mu}{\sigma}\right)^2} \right) (1-p)(1-p) \\
&+ \left(\frac{1}{\sqrt{2\pi * (\sigma^2 + s^2)}} e^{-\frac{1}{2}\frac{(z_t-\mu-m)^2}{\sigma^2+s^2}} \right) p(1-p) \\
&+ \left(\frac{1}{\sqrt{2\pi * (\sigma^2 + s^2)}} e^{-\frac{1}{2}\frac{(z_t-\mu+m)^2}{\sigma^2+s^2}} \right) (1-p)p \\
&+ \left(\frac{1}{\sqrt{2\pi * (\sigma^2 + 2s^2)}} e^{-\frac{1}{2}\frac{(z_t-\mu)^2}{\sigma^2+2s^2}} \right) p^2.
\end{aligned} \tag{4.29}$$

With this probability density function, the parameters μ, σ, m, s , and p can be estimated by maximizing the logarithm of the likelihood function. The likelihood function, based on the observations $\{z_1, \dots, z_{T-1}\}$, is equal to:

$$L = \prod_{t=1}^{T-1} f(z_t). \tag{4.30}$$

The estimates of the parameters are consequently obtained by taking the logarithm of (4.30) and maximizing the function:

$$\begin{aligned}
\log L &= \log \prod_{t=1}^{T-1} f(z_t) = \sum_{t=1}^{T-1} \log f(z_t) \\
&= \sum_{t=1}^{T-1} \log \left(\left(\frac{1}{\sigma\sqrt{2\pi}} e^{-\frac{1}{2}\left(\frac{z_t-\mu}{\sigma}\right)^2} \right) (1-p)(1-p) \right. \\
&+ \left(\frac{1}{\sqrt{2\pi * (\sigma^2 + s^2)}} e^{-\frac{1}{2}\frac{(z_t-\mu-m)^2}{\sigma^2+s^2}} \right) p(1-p) \\
&+ \left(\frac{1}{\sqrt{2\pi * (\sigma^2 + s^2)}} e^{-\frac{1}{2}\frac{(z_t-\mu+m)^2}{\sigma^2+s^2}} \right) (1-p)p \\
&\left. + \left(\frac{1}{\sqrt{2\pi * (\sigma^2 + 2s^2)}} e^{-\frac{1}{2}\frac{(z_t-\mu)^2}{\sigma^2+2s^2}} \right) p^2 \right).
\end{aligned} \tag{4.31}$$

Next, the parameters c_0 and c_1 from (4.27) need to be estimated in order to construct forecasts for the time series and eventually for the central death rates and death probabilities.

According to Kendall and Ord (1990), autoregressive models, just like the one

in (4.27) can be estimated using OLS. The lags of the time-series will be used as independent variables to obtain estimates for c_0 and c_1 .

4.4.3 Closure method of Kannisto

Due to the limited number of observations for mortality for ages above 90, a different method should be applied to obtain estimates for these numbers. To obtain estimates for $\mu_{x,t}^{g,NL}$ for ages above 90, the Kannisto (1992) method is applied, following a similar approach as the models developed by the AG. Kannisto's method extrapolates the estimates $\mu_{x,t}^{g,NL}$ from ages 80-90, to obtain estimates for $\mu_{x,t}^{g,NL}$ for the ages 91-120. This is referred to as the closure of the mortality table. Using a logistic regression based on the estimates for $\mu_{x,t}^{g,NL}$ for the ages 80-90, the model is extrapolated. The AG2020 and earlier models from the AG used this method as well. However, in the AG2022 model, while still applying Kannisto, the method described in 4.3.1 is employed.

The closure of the mortality table is obtained by:

$$\mu_{x,t}^{g,NL} = L\left(\sum_{k=1}^n w_k(x)L^{-1}(\mu_{y_k}(t))\right). \quad (4.32)$$

In this context, L represents the logistic function and L^{-1} denotes the inverse logistic function,

$$L(x) = \frac{1}{1 + e^{-x}} \quad (4.33)$$

$$L^{-1}(x) = -\log\left(\frac{1}{x} - 1\right) \quad (4.34)$$

with regression weights $w_k(x)$ equal to:

$$w_k(x) = \frac{1}{n} + \frac{(y_k - \bar{y})(x - \bar{y})}{\sum_{j=1}^k (y_j - \bar{y})^2} = \frac{1}{11} + \frac{(y_k - 85)(x - 85)}{110}. \quad (4.35)$$

Here, $y_k = 79 + k$, for $k = \{1, \dots, 11\}$, $\bar{y} = 85$, which is the average of the ages $\{80, \dots, 90\}$, and $\sum_{j=1}^k (y_j - \bar{y})^2 = 110$ is the squared sum of deviations.

From an econometric point of view the following approach can also be used: First, use OLS to estimate

$$L^{-1}(\mu_{x,t}^{g,NL}) = \beta_0 + \beta_1 x + \epsilon, \quad x \in \{80, \dots, 90\}. \quad (4.36)$$

Then, use the obtained estimates $\hat{\beta}_0$ and $\hat{\beta}_1$ to find the values for $L^{-1}(\mu_{x,t}^{g,NL})$ for ages $x \in \{91, \dots, 120\}$.

$$L^{-1}(\mu_{y,t}^{g,NL}) = \hat{\beta}_0 + \hat{\beta}_1 y, \quad y \in \{91, \dots, 120\}. \quad (4.37)$$

Next, values for $\mu_{y,t}^{g,NL}$ for ages $y \in \{91, \dots, 120\}$ can be obtained by:

$$\mu_{y,t}^{g,NL} = L(\hat{\beta}_0 + \hat{\beta}_1 y). \quad (4.38)$$

Substituting the expressions for the OLS estimates $\hat{\beta}_0$ and $\hat{\beta}_1$ into (4.38) yields (4.32)

5 Results

In this chapter the results of the model introduced in Chapter 4.4 are discussed. Using the data described in Chapter 3, a multi-population mortality model incorporating mortality shocks is calibrated and forecasted. The parameters are estimated, an outlier analysis is conducted and forecasted mortality scenarios are created. Furthermore, a sensitivity analysis is conducted on the model by using a different calibration period for estimating the parameters. In this chapter the superscript $g = \{F, M\}$ is re-introduced in the parameters A_x^g , B_x^g , K_t^g , $\alpha_x^{g,NL}$, $\beta_x^{g,NL}$, and $\kappa_t^{g,NL}$ from (4.19) for distinguishing genders.

5.1 Benchmark model

The first results in this chapter are based on the benchmark model. This model is calibrated on the countries in \mathcal{I} , on the calibration period $\mathcal{T} = \{1900, \dots, 2021\}$, for ages $\mathcal{X} = \{0, \dots, 90\}$.

5.1.1 Parameter estimation

After calibrating the parameters on the given calibration period, as described in 4.4.1, the estimates \hat{A}_x^g , \hat{B}_x^g , \hat{K}_t^g , $\hat{\alpha}_x^{g,NL}$, $\hat{\beta}_x^{g,NL}$, and $\hat{\kappa}_t^{g,NL}$ from (4.19) are obtained. Recall that A_x^g depicts the age-specific evolution of the mortality trend, B_x^g denotes the age specific sensitivity to changes in K_t^g , and K_t^g is the time-varying mortality index. $\alpha_x^{g,NL}$, $\beta_x^{g,NL}$, and $\kappa_t^{g,NL}$ respectively have the same definitions, but are the country specific deviations from the European reference group. In this model, this is the deviation of the Netherlands from the European reference group. Figure 5.1 depicts the age-dependent parameter estimations of \hat{A}_x^g , \hat{B}_x^g , $\hat{\alpha}_x^{g,NL}$, and $\hat{\beta}_x^{g,NL}$ for both males and females.

Additionally, the estimates of the time-varying parameters \hat{K}_t^g and $\hat{\kappa}_t^{g,NL}$ are depicted in Figure 5.2.

From the evolution of A_x^g it is visible that it declines rapidly from age 0 to age 1, meaning that the mortality trend for newborns is a lot higher compared to individuals reaching the age 1 or higher. Afterwards the mortality trend gradually increases again, showing that the mortality trend increases with age, which is a logical inference. The hump around age 20 for males may be attributed to the risk-taking behavior of young adults, leading to accidental deaths. This humps is also known as the accident hump, and mostly has impact on young adult males. From the evolution of K_t^g it is clearly visible that mortality is in a declining trend over the years. This aligns with the fact that from 1900 onwards, life expectancy is in an increasing trend. The upward

spikes denote the first World War in combination with the Influenza pandemic, and the second World War. Also, a small jump upwards in 2020 occurred due to the Covid-19 pandemic.

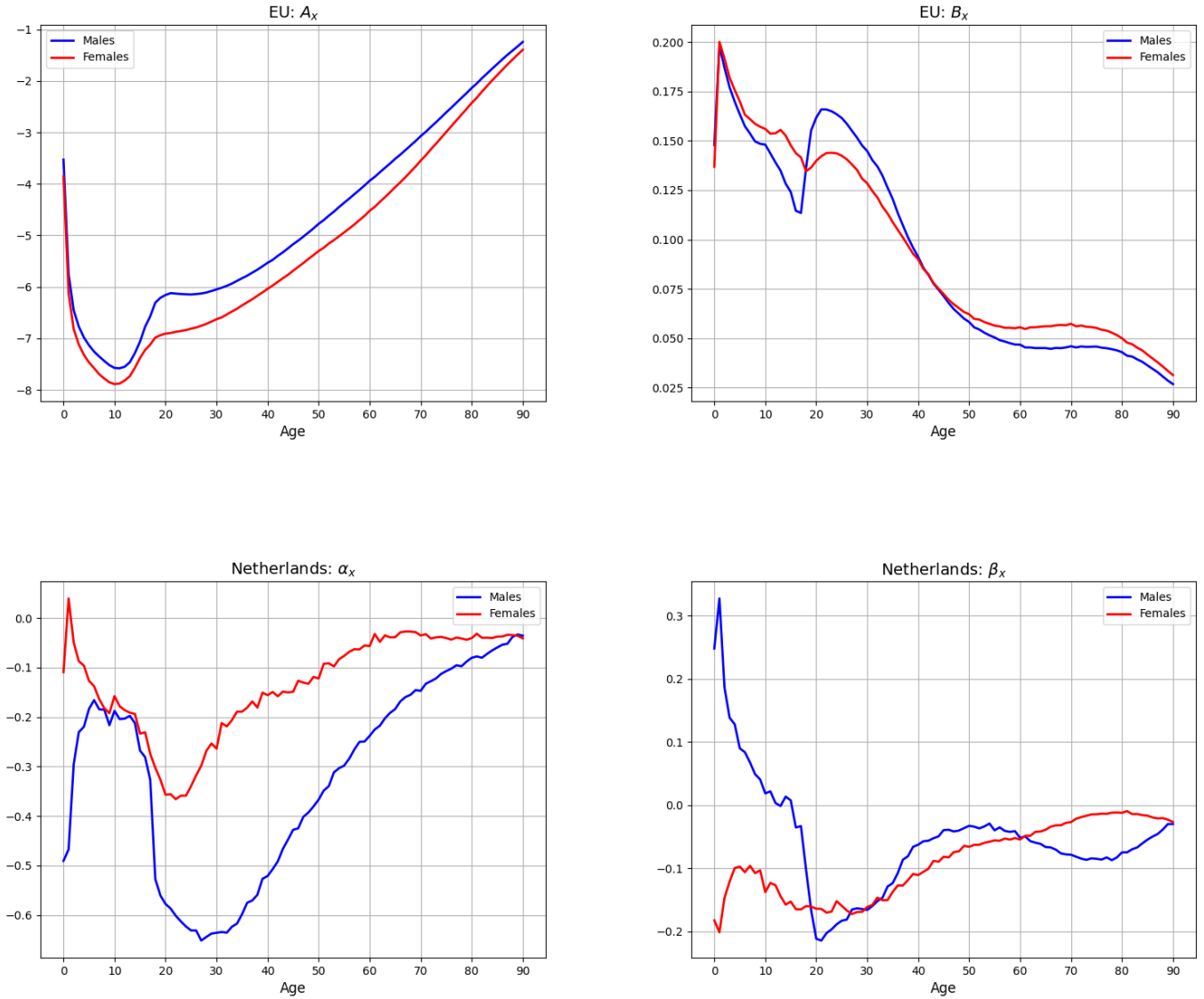


Figure 5.1: Estimation of the age-specific parameters \hat{A}_x and \hat{B}_x for the European reference group and estimation of the age-specific parameters $\hat{\alpha}_x^{g,NL}$ and $\hat{\beta}_x^{g,NL}$ for the Dutch deviation for ages 0-90 in years 1900-2021. Note, for obtaining a unique solution while estimating the parameters, four normalizations were introduced: $\sum B_x^2 = 1$, $\sum \beta_x^2 = 1$, $\sum K_t = 0$ and $\sum \kappa_t = 0$

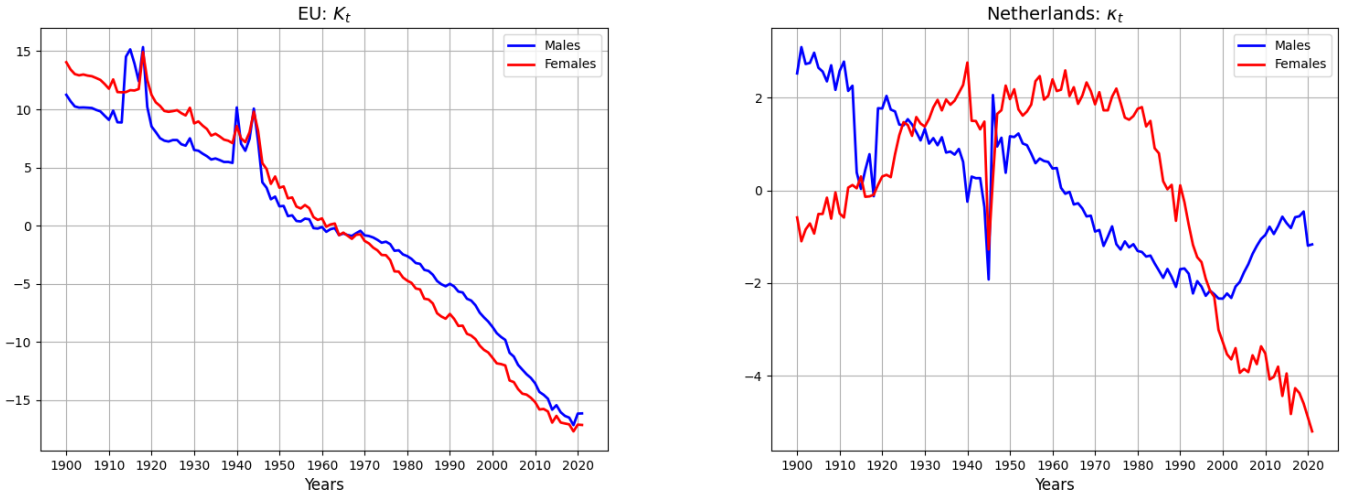


Figure 5.2: Estimation of the mortality index \hat{K}_t^g for the European reference group and its Dutch deviation $\hat{\kappa}_t^g$ for ages 0-90 in years 1900-2021. Note, for obtaining a unique solution while estimating the parameters, four normalizations were introduced: $\sum B_x^2 = 1$, $\sum \beta_x^2 = 1$, $\sum K_t = 0$ and $\sum \kappa_t = 0$. The graph for $\hat{\kappa}_t^g$ may appear volatile, however, when comparing the y-axis of the two graphs, the Dutch deviation compared to the European reference group is not significantly large.

5.1.2 Outlier analysis

By using the method described in Chapter 4.4.2, Z-scores are calculated and outliers are obtained in the evolution of K_t^g . Differencing is applied to obtain values for ΔK_t^g for each year. Figure 5.3 and Figure 5.4 depict the observed outliers for females and males respectively. The threshold for the analysis of the Z-scores for females is 1.2 standard deviations from the mean. For males this is 1 standard deviation. Everything above that threshold is considered an outlier. Most of the values of ΔK_t^g are negative, because the evolution of K_t^g has a downward trend, as depicted in figure 5.2. The upward spikes indicate a jump in the mortality index K_t^g , therefore only the upward spikes are considered as outliers.

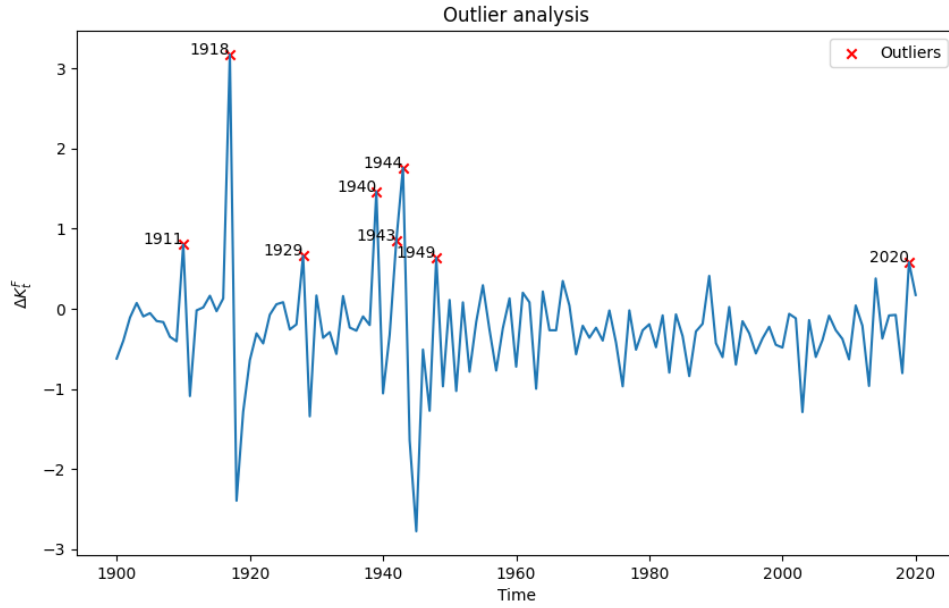


Figure 5.3: Outlier analysis for the European female population's mortality index K_t^F . Using differencing, ΔK_t^F is obtained for each year. The figure highlights the timing of the outliers with a red cross.

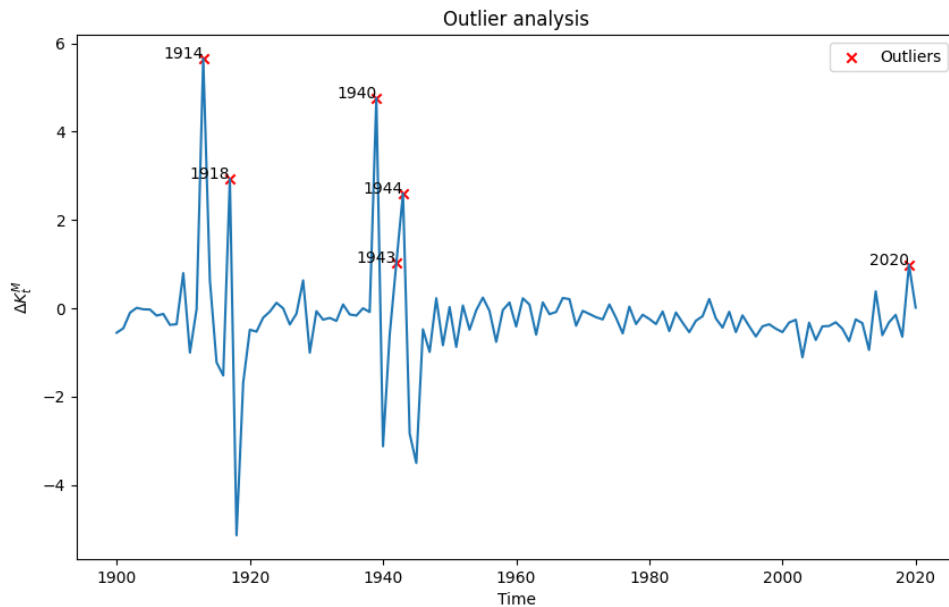


Figure 5.4: Outlier analysis for the European male population's mortality index K_t^M . Using differencing, ΔK_t^M is obtained for each year. The figure highlights the timing of the outliers with a red cross.

For both females and males, the timing of the most severe outliers align with the timing of the First World War (1914-1918), the influenza pandemic (1918) and the Second World War (1939-1945) in the European reference group. These catastrophic events lead to severe mortality shocks in the European population. Furthermore, the female population also shows some smaller outliers in other years in the first half of the twentieth century.

The Covid-19 pandemic in 2020 is the reason for the first outlier in a period of more than 70 years without an outlier. For both females and males, the spike in the mortality trend K_t^g is large enough, given the chosen threshold, to be considered an outlier.

The results of the outlier analysis indeed show the existence of outliers in the mortality index K_t^g . This underscores the necessity of incorporating jumps in mortality models. Consequently, in the next section future scenarios of mortality are generated while including a jump process in the model.

5.1.3 Forecasted mortality scenarios

Recall from Chapter 4.4.2 that:

$$K_t = K_{t-1} + \mu + \sigma Q_t + N_t Y_t - N_{t-1} Y_{t-1}, \quad (5.1)$$

where N_t represents the indicator of whether a mortality shock occurred in year t , and the probability of a shock event is p . The severity of the shock is measured by Y_t . It is assumed that Y_t is an identically independently normally distributed variable with mean m and standard deviation s . μ is the constant drift term, σ is the constant error term and Q_t is a standard normal variable. Table 5.1 shows the estimates of the parameters for the time-series.

Parameter	Female	Male
μ	-0.237 (0.038)	-0.253 (0.034)
σ	0.265 (0.055)	0.308 (0.034)
p	0.183 (0.071)	0.086 (0.026)
m	0.000 (0.787)	0.882 (3.437)
s	0.981 (0.207)	2.426 (1.170)

Table 5.1: Estimated parameters of the time series for K_t^g with the standard error between brackets, for the calibration period 1900-2021. The estimates are obtained using the Log-Likelihood maximization described in Chapter 4.

For comparison, Table 5.2 presents the estimates for the parameters in (4.24), the time-series for the overall mortality trend without a jump component.

Parameter	Female	Male
μ	-0.258 (0.038)	-0.226 (0.034)
σ	0.436 (0.128)	1.222 (0.351)

Table 5.2: Estimated parameters of the time series for $\tilde{K}_t = \mu + \tilde{K}_{t-1} + \sigma Q_t$, which is K_t^g without jump component. Standard error between brackets, for the calibration period 1900-2021.

Table 5.2 shows higher values for the volatility term σ than in Table 5.1. Because all the shocks in K_t^g are now incorporated in the volatility term rather than in the additional jump term, I find higher values for σ , particularly for males. Moreover, the values for μ slightly differ. The omission of m , the parameter that measures the mean of the shock, has an effect on this difference. Both upward and downward shocks are now incorporated in μ , resulting in different estimates.

Also recall from Chapter 4.4.2 that:

$$\kappa_t^{NL} = c_0 + c_1\kappa_{t-1}^{NL} + \sigma_\delta\delta_t, \quad (5.2)$$

where c_0 and c_1 are parameters of the time series, σ_δ is the error term and δ_t is a standard normal variable. The estimates of these parameters are depicted below in Table 5.3.

Parameter	Female	Male
c_0	-0.004 (0.054)	0.005 (0.059)
c_1	0.965 (0.024)	0.908 (0.039)
σ	0.596 (0.083)	0.656 (0.096)

Table 5.3: Estimated parameters of the time series for κ_t^g with the standard error between brackets, for the calibration period 1900-2021. The estimates are obtained using OLS as described in Chapter 4.

Using the estimates from Table 5.1 and Table 5.3, future mortality scenarios can be simulated. First, the time series for both K_t^g and κ_t^g can be estimated for periods after $t = 2021$. Simulating 100,000 scenarios for the evolution of K_t^g and κ_t^g for both genders lead to the plots in Figure 5.5 and Figure 5.6. The median forecasts and the 90% confidence intervals of the future evolutions of K_t^g and κ_t^g are depicted. Furthermore, the estimates from Table 5.2 are used to depict a confidence interval for the forecasts when shocks are not incorporated. i.e. when (4.24) is used to model the evolution of K_t^g instead of (4.26).

The future evolutions for K_t^M show a wider confidence interval compared to the the future evolutions for K_t^F . The estimates of the parameters presented in Table 5.1 show larger numbers for σ and s for males compared to females. This implies that the evolution of the time-series will be more volatile, leading to a wider confidence interval. For females, the confidence interval of the model without shocks is slightly smaller compared to the confidence interval for the model with shocks. However, for males there is a large difference in the confidence intervals. The reason for this is the difference in σ in Table 5.1 and Table 5.2. The mortality shocks thus have a large impact on the forecasts.

The confidence interval for the evolution of κ_t^F and κ_t^M in Figure 5.6 appear to be concentrated around 0. This indicates that the future evolution of the European mortality trend aligns with the Dutch future mortality trend.

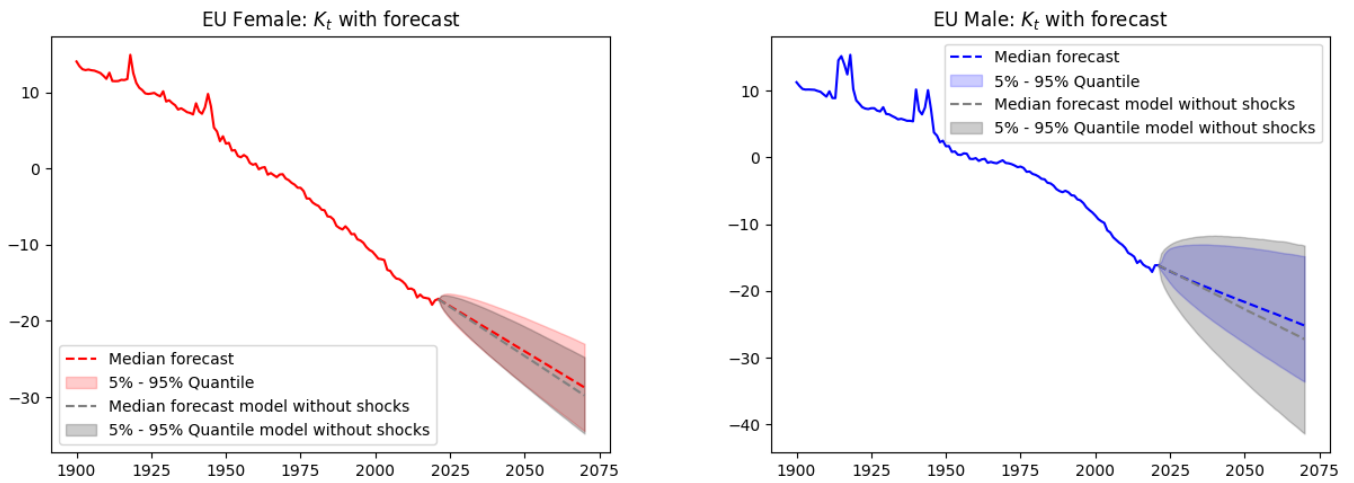


Figure 5.5: time-series for K_t for females (left) and males (right) for ages 0-90 in years 1900-2021. 100,000 simulations of the future evolution are produced for ages 0-90 in years 2022-2070. The median and the 90% confidence interval for these simulations are depicted. Furthermore, the confidence interval for the forecasts of the model without shocks are presented.

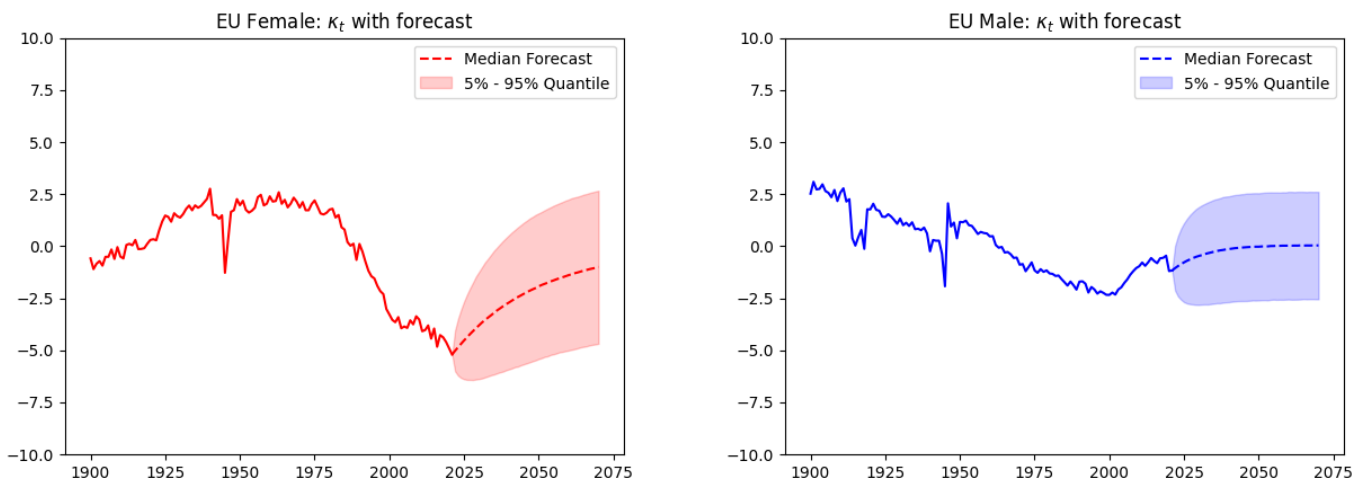


Figure 5.6: time-series for $\kappa_t^{g,NL}$ for females (left) and males (right) for ages 0-90 in years 1900-2021. 100,000 simulations of the future evolution are produced for ages 0-90 in years 2022-2070. The median and the 90% confidence interval for these simulations are depicted.

The evolution of K_t^g gives insights in future mortality trends, but does not give meaningful numerical values. Mortality tables or death probabilities are more appropriate to give a more sensible meaning to the numbers. With the obtained estimates \hat{A}_x^g , \hat{B}_x^g , \hat{K}_t^g , $\hat{\alpha}_x^{g,NL}$, $\hat{\beta}_x^{g,NL}$ and $\hat{\kappa}_t^{g,NL}$ for ages $x \in \mathcal{X} = \{0, \dots, 90\}$ in years $t \in \mathcal{T} = \{1900, \dots, 2021\}$, and with the simulated values for \hat{K}_x^g and $\hat{\kappa}_t^{g,NL}$ for the years $\{2022, \dots, 2070\}$, mortality tables for both genders can be produced.

Based on (4.19), the estimates $\hat{\mu}_{x,t}^{g,NL}$ for ages 0-90 in years 1900-2070 can be modeled. Then using the method by Kannisto (1992), as described in Chapter 4.4.3, the estimates $\hat{\mu}_{x,t}^{g,NL}$ can be extrapolated for ages 91-120.

Recall that the death probabilities can be calculated by:

$$q_{x,t}^g = 1 - e^{-\hat{\mu}_{x,t}^{g,NL}}. \quad (5.3)$$

The obtained estimates $\hat{\mu}_{x,t}^{g,NL}$ for ages 0-120 in years 1900-2070 can now be translated to death probabilities using (5.3).

Figure 5.7 depicts the calibration $q_{x,t}^F$ for ages $x \in \{20, 40, 60, 80\}$ and Figure 5.8 depicts the corresponding calibration for males ($q_{x,t}^M$). The figures depict the fitted values for $q_{x,t}^g$ in $t = \{1900, \dots, 2021\}$ and the observed mortality rates in the same time period, obtained from the HMD (2023). Furthermore, the figures depict the simulated values for $q_{x,t}^g$ in the years $t = \{2022, \dots, 2070\}$ with a 99 % confidence interval. The red line is a reference line with forecast estimates of $q_{x,t}^g$ by the AG2022 model (AG, 2022) for the years $t = \{2022, \dots, 2070\}$.

Figure 5.7 and Figure 5.8 focus specifically on the period 1970-2070. This is done because it shows the death probabilities for the recent past and near future. The zoomed-out figures, depicting the death probabilities for the period 1900-2070, can be found in appendix A.

The fitted values and the observed values for $q_{x,t}^g$ in all eight graphs seem to have a downward trend. This aligns with the increasing trend in life expectancy. For the graphs on female death probabilities, the AG2022 forecast fits well within the 99 % confidence interval for the forecasts of the multi-population mortality model with shocks. Except, for a few values at higher ages around the year 2021, likely influenced by the Covid-19 pandemic, the estimates of the AG2022 model do not fit within the confidence interval.

In case of the male death probabilities, a clear difference is observed when comparing the AG2022 model with the multi-population mortality model incorporating shocks. The AG2022 model predicts higher death probabilities for ages 20 and 40, and lower death probabilities for age 60. For age 80, the AG2022 has a steeper downward slope, this could occur because the AG2022 model adds a big shock for older age groups because of the Covid-19 pandemic. A reason for these differences could be the different calibration periods between the the multi-population model incorporating shocks and the AG2022 model. The multi-population model incorporating shocks covers a more extended calibration period from 1900 to 2021. Shocks that occurred before 1970 could have an impact on the death probabilities later on. In contrast, the AG2022 model has a shorter calibration period from 1970 to 2020, potentially leading to differences in predicted death probabilities. Despite these differences, the

AG2022 model generally fits within the confidence interval as forecasted by the multi-population mortality model incorporating shocks.

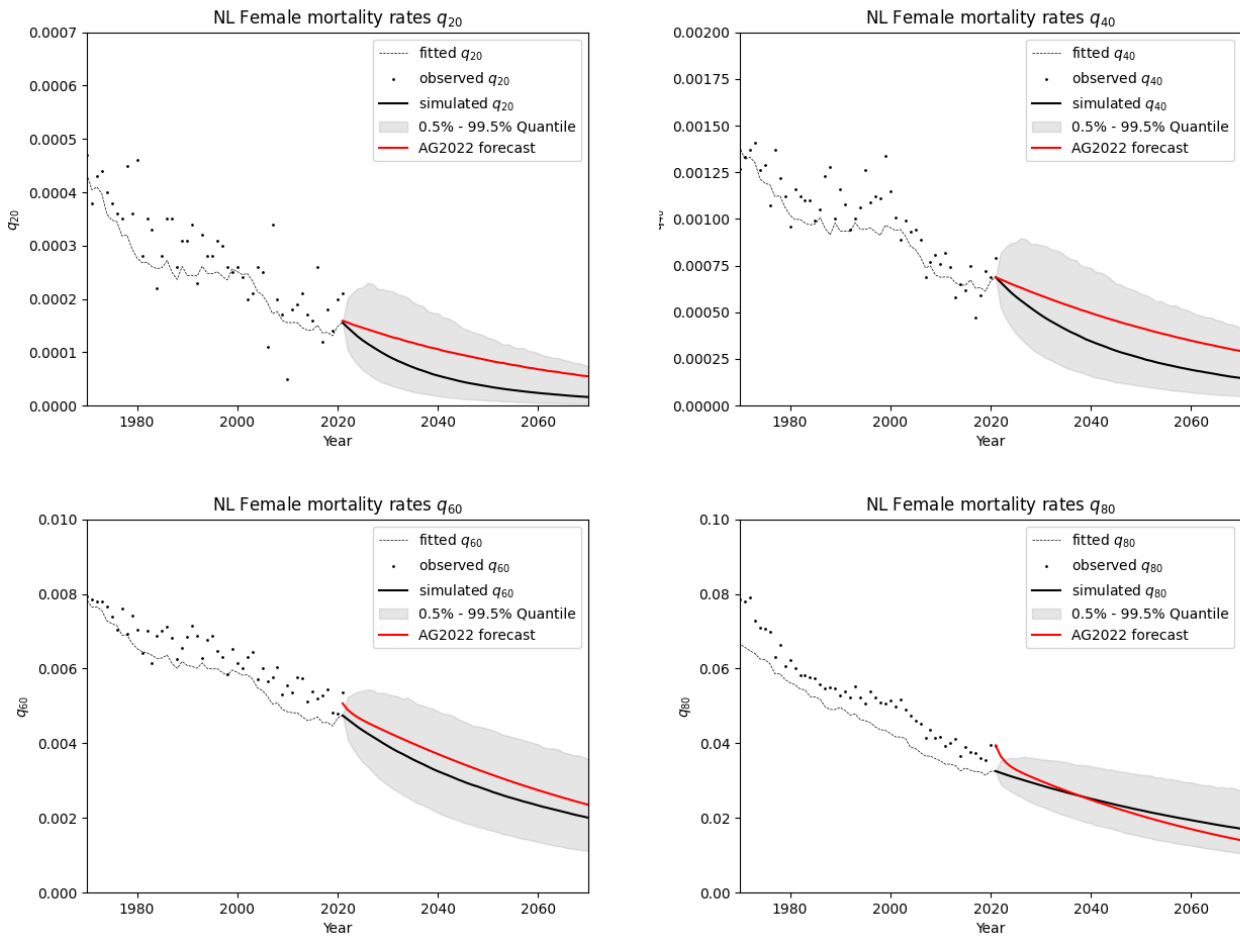


Figure 5.7: Estimates, observed values, and forecasts for death probabilities for ages 20, 40, 60, and 80 for Dutch females, zoomed in on 1970-2070. Calibration period 1900-2021, and projection 2022-2070. The median and the 99% confidence interval obtained from 10,000 simulations are plotted. As a reference, the AG2022 forecast is added as well.

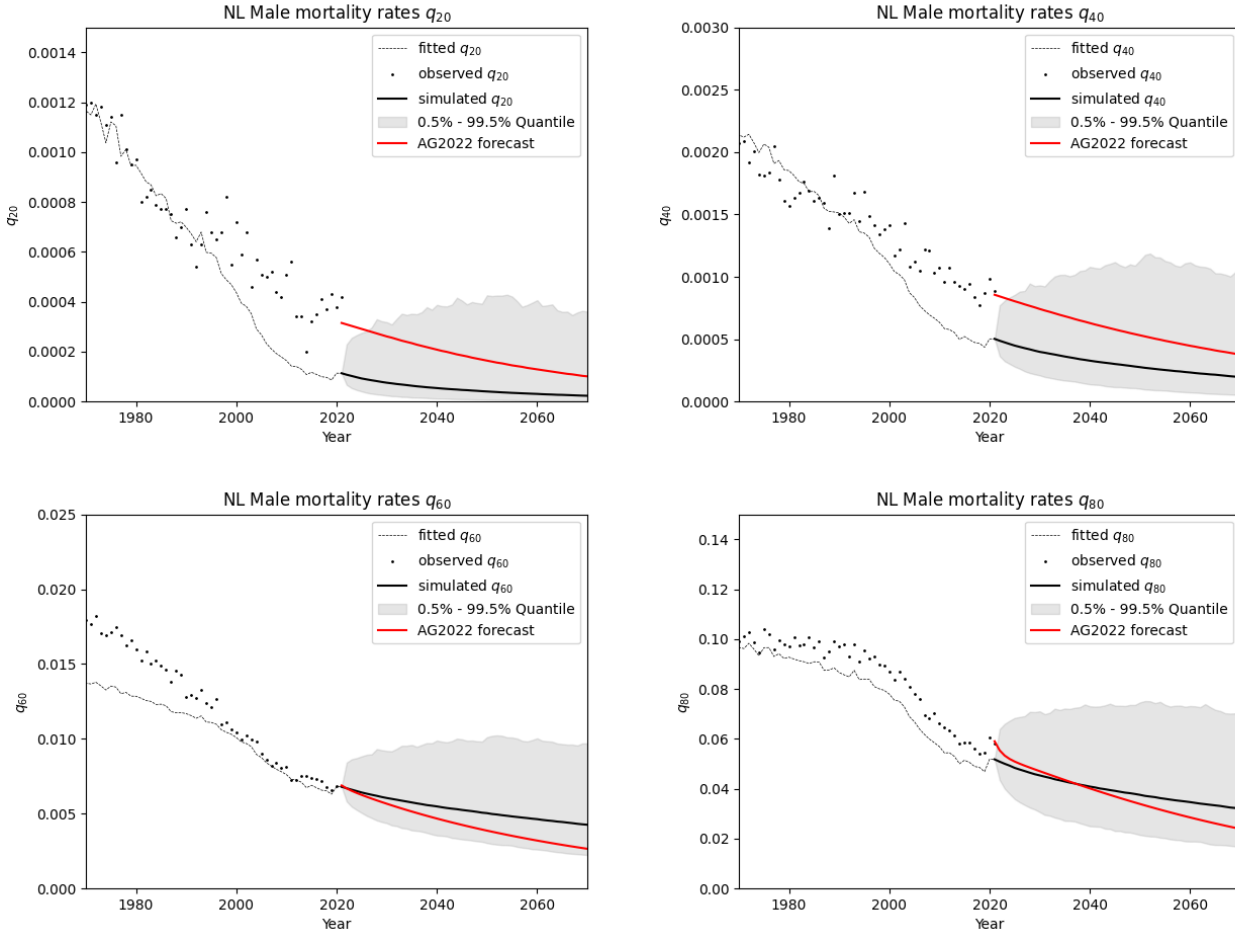


Figure 5.8: Estimates, observed values, and forecasts for death probabilities for ages 20, 40, 60, and 80 for Dutch males, zoomed in on 1970-2070. Calibration period 1900-2021, and projection 2022-2070. The median and the 99% confidence interval obtained from 10,000 simulations are plotted. As a reference, the AG2022 forecast is added as well.

Having obtained estimates and forecasts for the death probabilities $q_{x,t}^g$, for ages 0-120 and years 1900-2070, life expectancies can be computed.

Period life expectancy is calculated by (AG, 2022):

$$e_{x,t}^{g,per} = \frac{1}{2} + \sum_{k=0}^{\infty} \prod_{s=0}^k (1 - q_{x+s,t}^g). \quad (5.4)$$

Cohort life expectancy is calculated by (AG, 2022):

$$e_{x,t}^{g,coh} = \frac{1}{2} + \sum_{k=0}^{\infty} \prod_{s=0}^k (1 - q_{x+s,t+s}^g). \quad (5.5)$$

For calculating cohort life expectancies, scenarios of mortality beyond 2070 are necessary. More specifically, mortality scenarios until 2190 are necessary to obtain cohort life expectancies for an individual born in 2070. These mortality

scenarios are obtained using the same method as before. Figure 5.4 depicts the observed period life expectancy (HMD, 2023), and the model-fitted period life expectancy for a 0-year old, calibrated on the period 1900-2021 for both females and males. The graph also depicts the best estimate period life expectancy and its 95% confidence interval for the period 2022-2070. As a reference, the period life expectancy as forecasted by the AG2022 model, for the period 2022-2070 is added as well. Figure 5.5 depicts the cohort life expectancy and its 95% confidence interval for a 0-year old across the years 1970-2070 for both females and males. The figures depicting period and cohort life expectancies for the complete time periods from 1900 to 2021 can be found in Appendix A.

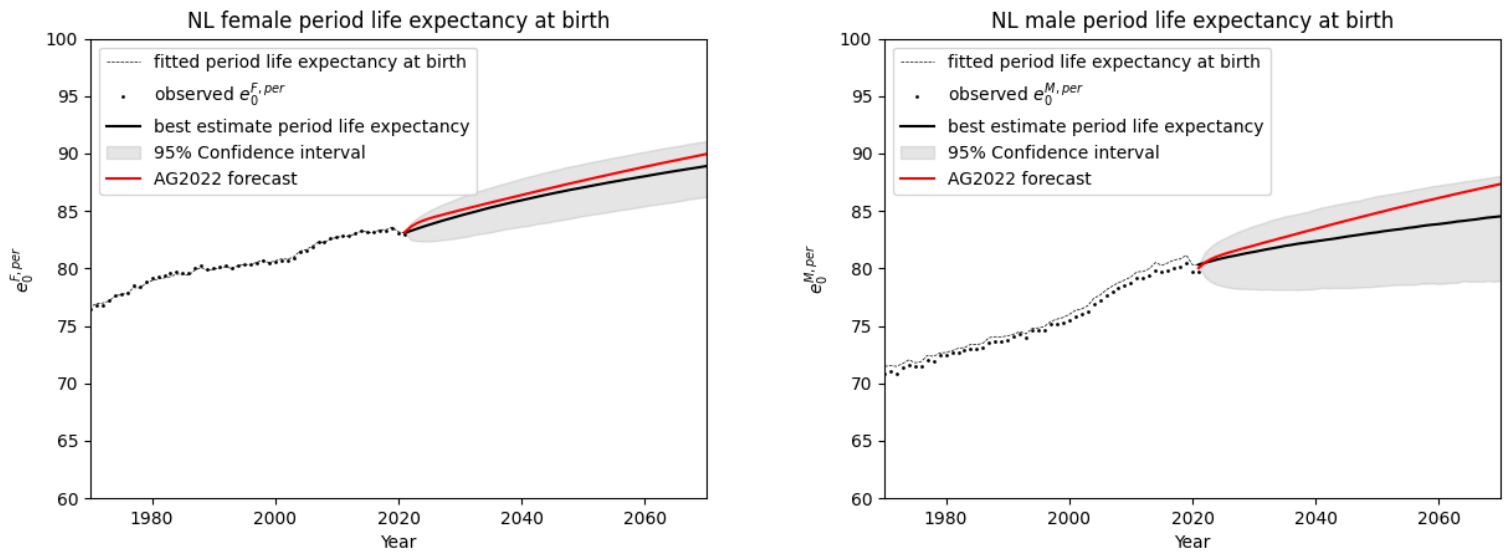


Figure 5.9: Observed and fitted period life expectancy for females (left) and males (right), calibrated on the years 1900-2021 for ages 0-90, closed by Kanisto's method, zoomed in on 1970-2070. Period life expectancy forecasts and a 95 % confidence interval for the years 2022-2070 are added as well. The red reference line is the AG2022 period life expectancy forecast.

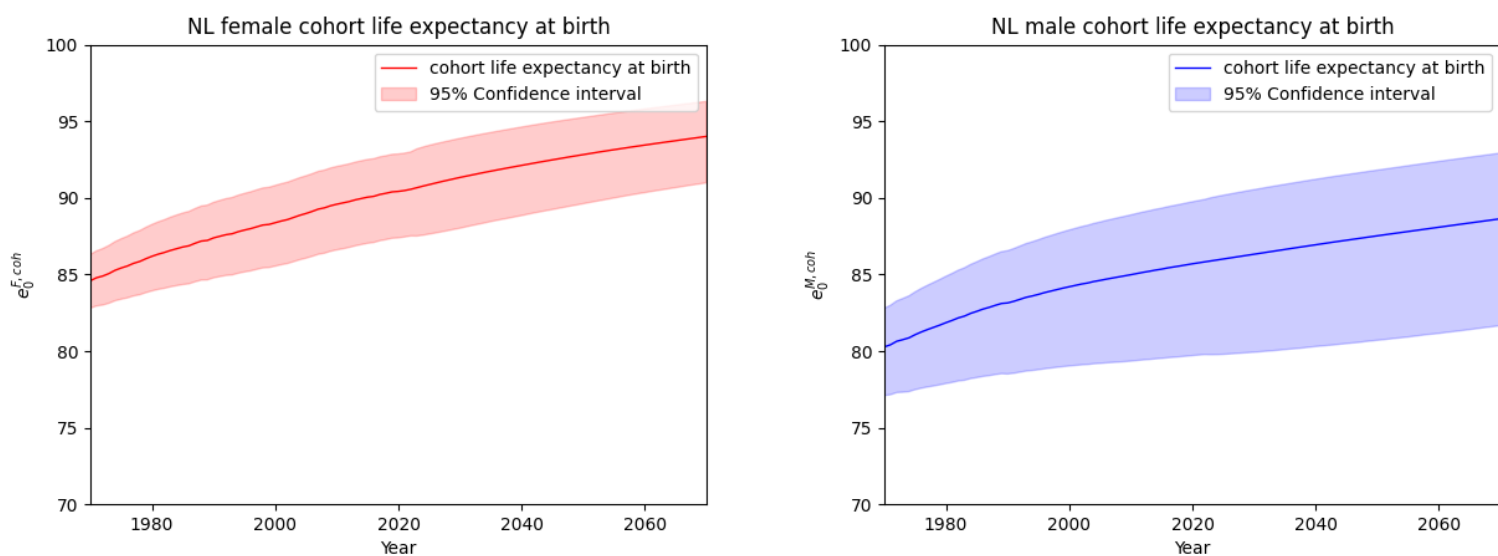


Figure 5.10: Fitted cohort life expectancy and its 95% confidence interval for females (left) and males(right), calibrated on the years 1900-2021 for ages 0-90, closed by Kannisto's method, zoomed in on 1970-2070.

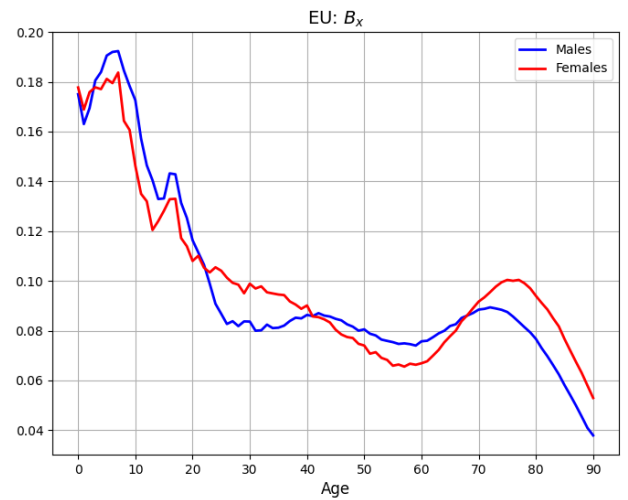
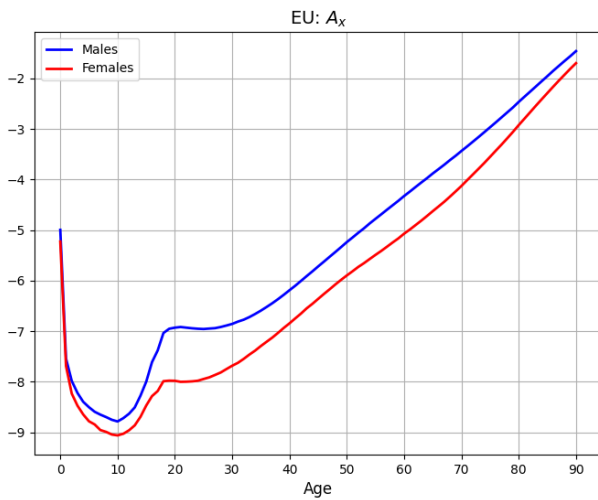
As depicted in Figure 5.9, the multi-population mortality model incorporating shocks underestimates the period life expectancies in future years, compared to the AG2022 model. The reason for this could again be that the multi-population mortality model incorporating shocks covers a more extended calibration period from 1900 to 2021. Shocks that occurred before 1970 could have an impact on the period life expectancies. Additionally, in both figures, the confidence intervals for males are wider than the female confidence intervals. The reason for this could be the more volatile evolution of the time-series for K_t^g and $\kappa_t^{g,NL}$ for males, leading to more volatile forecasts for period and cohort life expectancies, and therefore resulting in a wider confidence interval.

5.2 Sensitivity analysis

The previous section and its results are based on the benchmark model, calibrated on the countries in \mathcal{I} , on the calibration period $\mathcal{T} = \{1900, \dots, 2021\}$, for ages $\mathcal{X} = \{0, \dots, 90\}$. Next, a sensitivity analysis is conducted on a different calibration period. The sensitivity analysis will produce results based on the same model calibrated on the countries in \mathcal{I} , on the calibration period $\tilde{\mathcal{T}} = \{1970, \dots, 2021\}$, for ages $\mathcal{X} = \{0, \dots, 90\}$. The starting year of the calibration period is now equal to the starting year of the calibration period from the AG2022 model.

5.2.1 Parameter estimation

The estimates \hat{A}_x^g , \hat{B}_x^g , $\hat{\alpha}_x^{g,NL}$, and $\hat{\beta}_x^{g,NL}$ in Figure 5.11 show similar patterns as in the benchmark model. Figure 5.12 depicts the estimates \hat{K}_t^g and $\hat{\kappa}_t^{g,NL}$, which also show a similar trend as the benchmark, but over a shorter period (1970-2021). The difference of course is that the mortality shocks due to the two world wars and the Influenza pandemic are omitted during this period.



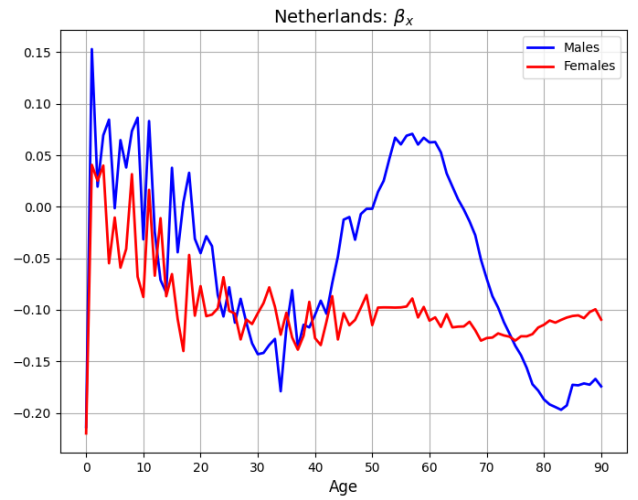
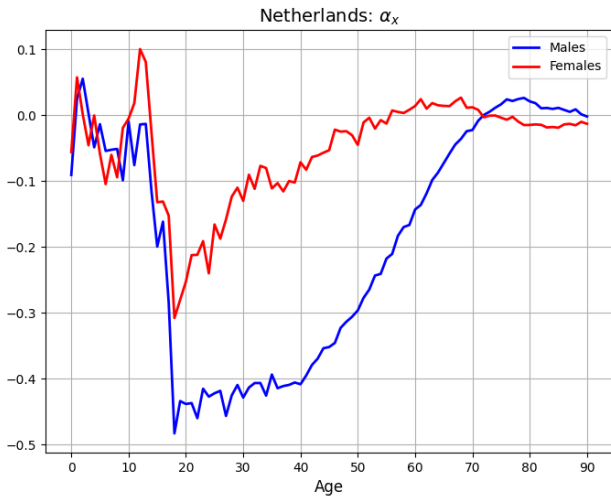


Figure 5.11: Estimation of the age-specific parameters \hat{A}_x and \hat{B}_x for the European reference group and estimation of the age-specific parameters $\hat{\alpha}_x^{g,NL}$ and $\hat{\beta}_x^{g,NL}$ for the Dutch deviation for ages 0-90 in years 1970-2021. Note, for obtaining a unique solution while estimating the parameters, four normalizations were introduced: $\sum B_x^2 = 1$, $\sum \beta_x^2 = 1$, $\sum K_t = 0$ and $\sum \kappa_t = 0$

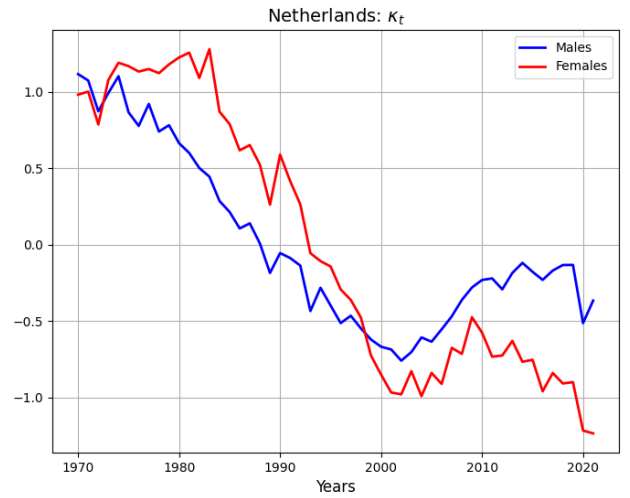
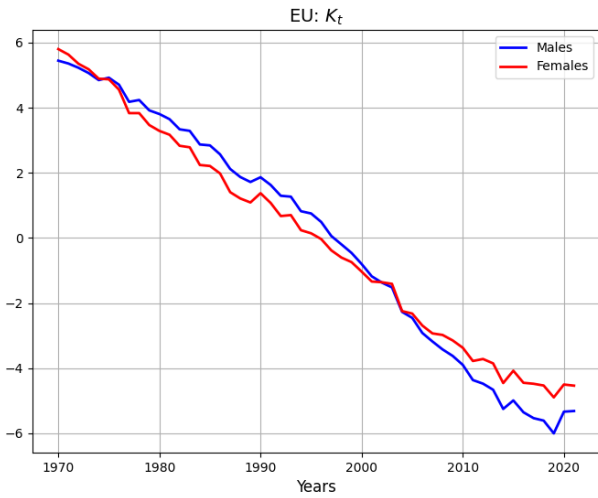


Figure 5.12: Estimation of the mortality index \hat{K}_t^g for the European reference group and its Dutch deviation $\hat{\kappa}_t^g$ for ages 0-90 in years 1970-2021. Note, for obtaining a unique solution while estimating the parameters, four normalizations were introduced: $\sum B_x^2 = 1$, $\sum \beta_x^2 = 1$, $\sum K_t = 0$ and $\sum \kappa_t = 0$. The graph for $\hat{\kappa}_t^g$ may appear volatile, however, when comparing the y-axis of the two graphs, the Dutch deviation compared to the European reference group is not significantly large.

5.2.2 Forecasted mortality scenarios

The different calibration periods lead to different estimates of the parameters for the time-series K_t^g and $\kappa_t^{g,NL}$. Compared to Table 5.1, the estimates for σ and s are smaller in Table 5.4. The evolution in the projected time-series for K_t therefore will be less volatile.

Parameter	Female	Male
μ	-0.191 (0.025)	-0.224 (0.026)
σ	0.143 (0.020)	0.159 (0.042)
p	0.082 (0.037)	0.064 (0.180)
m	0.485 (0.068)	0.331 (1.118)
s	0.000 (0.104)	0.298 (0.480)

Table 5.4: Estimated parameters of the time series for K_t^g with the standard error between brackets, for the calibration period 1970-2021. The estimates are obtained using the Log-Likelihood maximization described in Chapter 4.

Again, similar to Table 5.2, Table 5.5 presents the estimates for the parameters in (4.24), the time-series for the overall mortality trend without a jump component, now calibrated on 1970-2021.

Parameter	Female	Male
μ	-0.203 (0.025)	-0.211 (0.026)
σ	0.168 (0.074)	0.177 (0.089)

Table 5.5: Estimated parameters of the time series for $\tilde{K}_t = \mu + \tilde{K}_{t-1} + \sigma Q_t$, which is K_t^g , without shock. Standard error between brackets, for the calibration period 1970-2021.

The difference between σ in Table 5.4 and Table 5.5 is small compared to the difference in σ in the benchmark model. The fact that the mortality shocks before 1970 are not captured by the model anymore, contributes to this smaller difference. There still is a small difference in σ , due to the smaller mortality shocks in the period 1970-2021. These mortality shocks are all incorporated in the volatility term rather than in the additional jump term. Similar to the benchmark model, due to the omission of m , the values for μ slightly differ. Both upward and downward shocks are now incorporated in μ , resulting in different estimates.

The estimates of the time-series for $\kappa_t^{g,NL}$ in Table 5.6 do not show significant differences compared to the the estimates of the time-series in Table 5.3 from the benchmark model.

Parameter	Female	Male
c_0	0.000 (0.054)	0.001 (0.032)
c_1	0.917 (0.024)	0.909 (0.058)
σ	0.349 (0.039)	0.232 (0.043)

Table 5.6: Estimated parameters of the time series for κ_t^g with the standard error between brackets, for the calibration period 1970-2021. The estimates are obtained using OLS as described in Chapter 4.

Next, the forecasts for the time-series K_t and $\kappa_t^{g,NL}$ are depicted in Figure 5.13 and Figure 5.14 respectively.

The 90% confidence intervals in Figure 5.13 are narrower than the corresponding confidence intervals of the benchmark model in Figure 5.5. This is an effect of the less volatile parameters from the time-series for K_t . The confidence intervals for the model without shocks have similar width as the confidence intervals for the model with shocks now. A striking difference is the fact that, for females, the model without shocks leads to a lower forecast for K_t^F . Hence, incorporating shocks has a bigger effect on females than on males.

Again, similar to Figure 5.6, in Figure 5.14, the future evolution of $\kappa_t^{g,NL}$ are concentrated around 0. This indicates that the future evolution of the European mortality trend aligns with the Dutch future mortality trend.

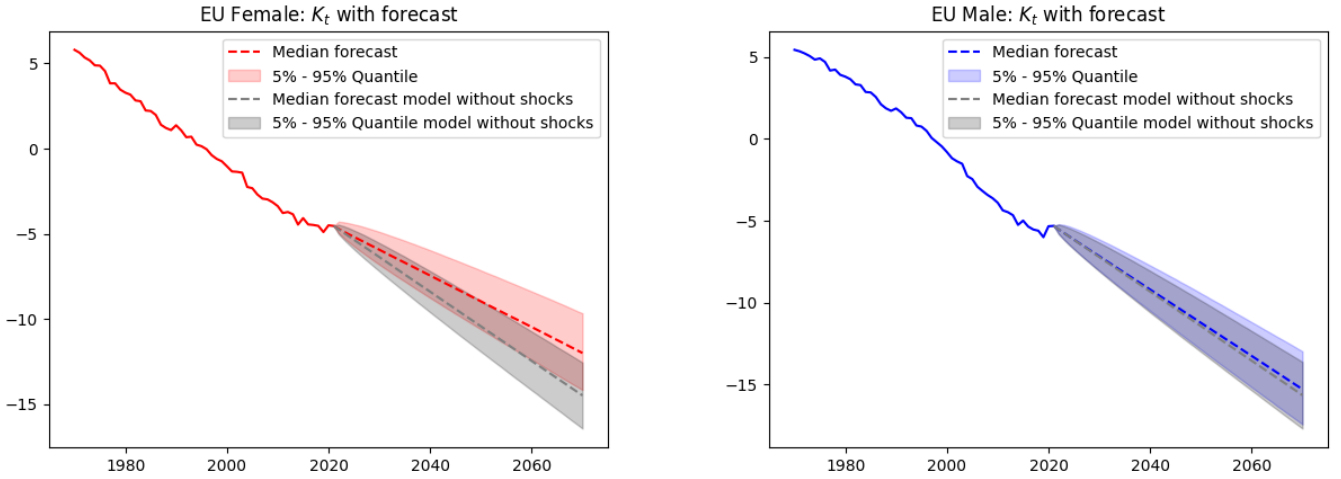


Figure 5.13: time-series for K_t for females (left) and males (right) for ages 0-90 in years 1970-2021. 100,000 simulations of the future evolution are produced for ages 0-90 in years 2022-2070. The median and the 90% confidence interval for these simulations are depicted. Furthermore, the confidence interval for the forecasts of the model without shocks are presented.

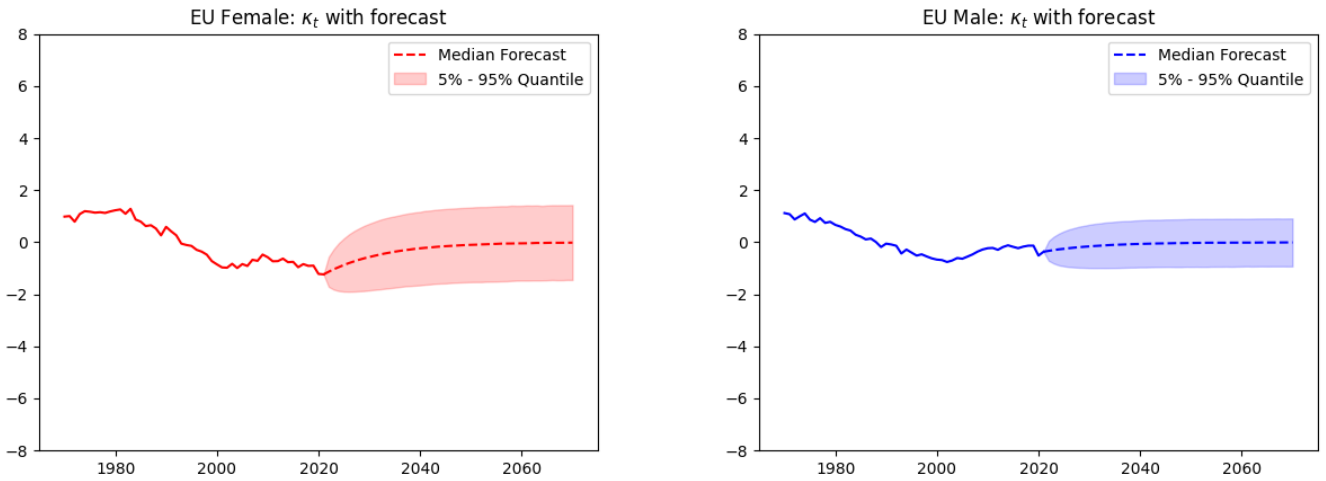


Figure 5.14: time-series for $\kappa_t^{g,NL}$ for females (left) and males (right) for ages 0-90 in years 1970-2021. 100,000 simulations of the future evolution are produced for ages 0-90 in years 2022-2070. The median and the 90% confidence interval for these simulations are depicted.

Next, new death probabilities are computed, based on the calibration period $\tilde{\mathcal{T}} = \{1970, \dots, 2021\}$. Figure 5.15 and Figure 5.16 depict the death probabilities $q_{x,t}^g$ for the model calibrated on the years 1970-2021 for ages $x \in \{20, 40, 60, 80\}$ for females and males respectively. The fitted values and the observed values are depicted for the period 1970-2021. The forecasted values with a 99% confidence interval and the reference by the AG2022 are depicted as well.

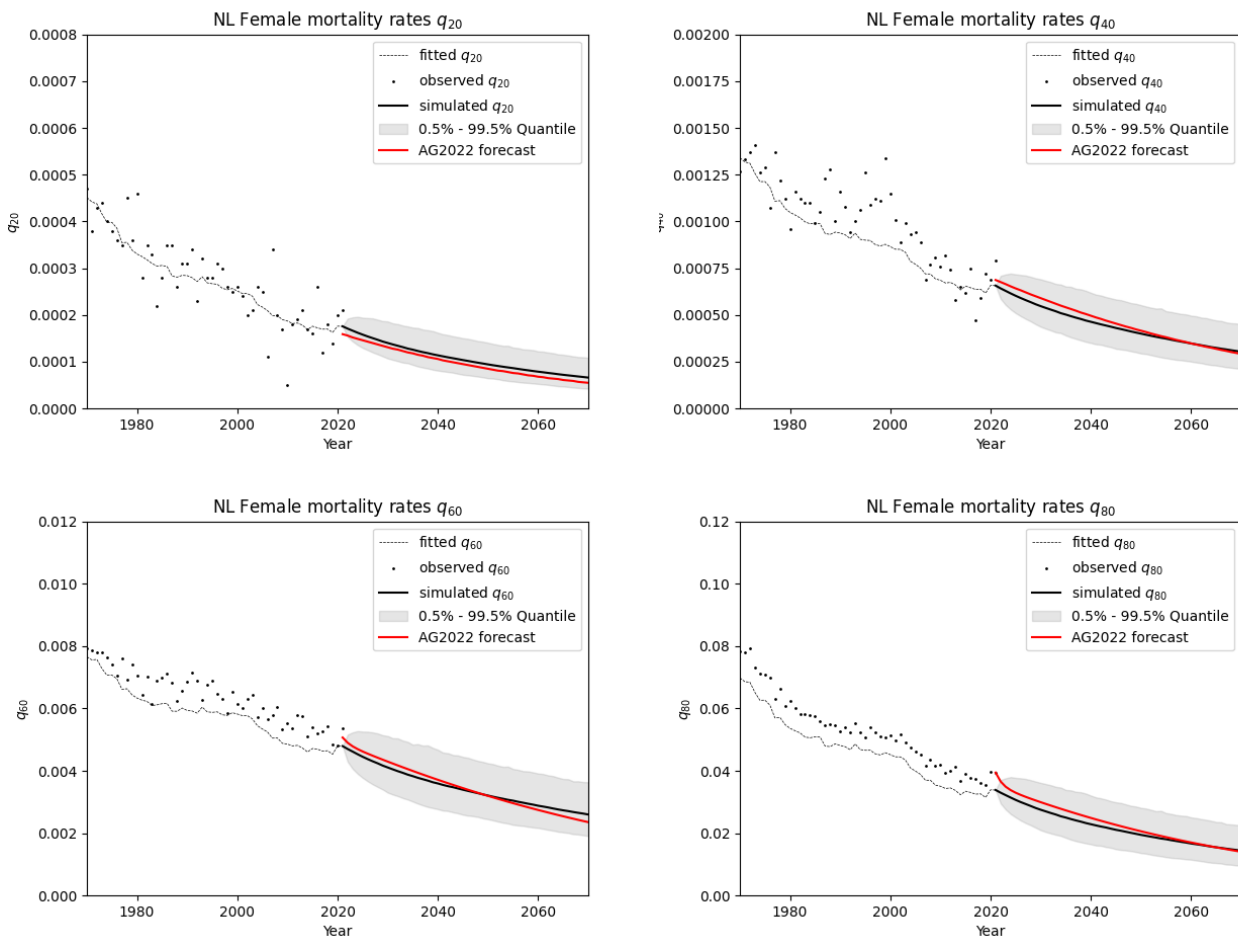


Figure 5.15: Estimates, observed values, and forecasts for death probabilities for ages 20, 40, 60, and 80 for Dutch females. Calibration period 1970-2021, and projection 2022-2070. The median and the 99% confidence interval obtained from 10,000 simulations are plotted. As a reference, the AG2022 forecast is added as well.

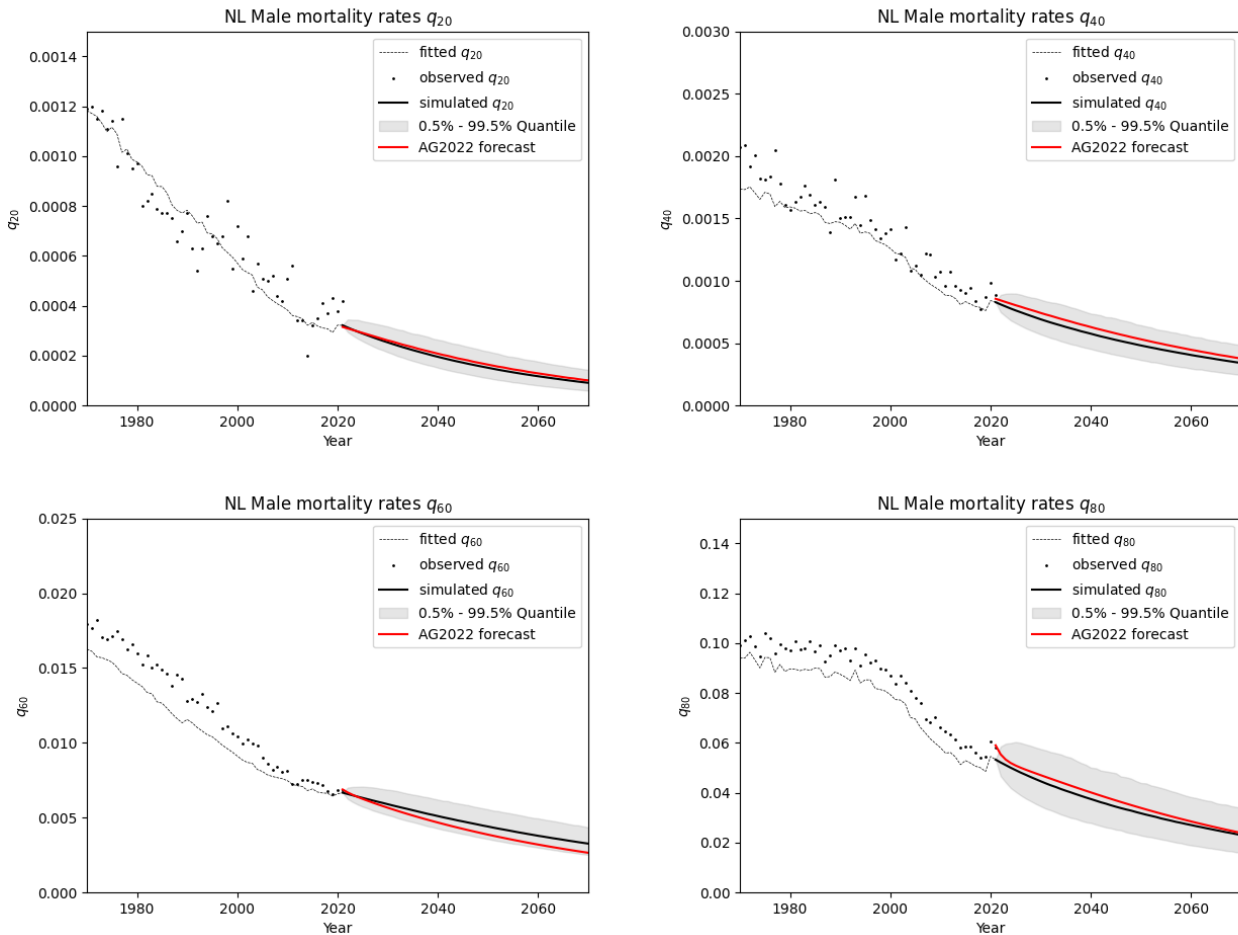


Figure 5.16: Estimates, observed values, and forecasts for death probabilities for ages 20, 40, 60, and 80 for Dutch males. Calibration period 1970-2021, and projection 2022-2070. The median and the 99% confidence interval obtained from 10,000 simulations are plotted. As a reference, the AG2022 forecast is added as well.

The new forecasted death probabilities are very close to the reference forecasted death probabilities by the AG2022 model. For both females and males, the AG2022 forecast almost completely fits within the 99% confidence interval. In addition, these confidence intervals are less wide than the confidence intervals in Figure 5.7 and 5.8 from the benchmark model.

Consequently, Figure 5.17 and Figure 5.18 depict the period and cohort life expectancy respectively, based on the new calibration period $\tilde{\mathcal{T}} = \{1970, \dots, 2021\}$.

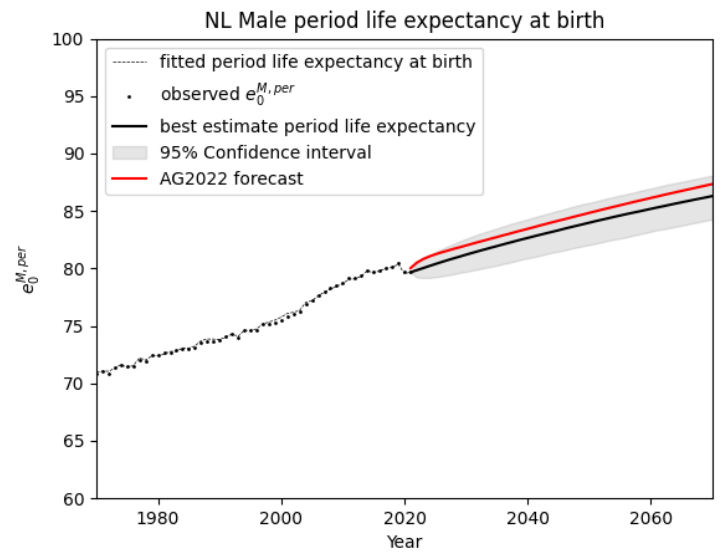
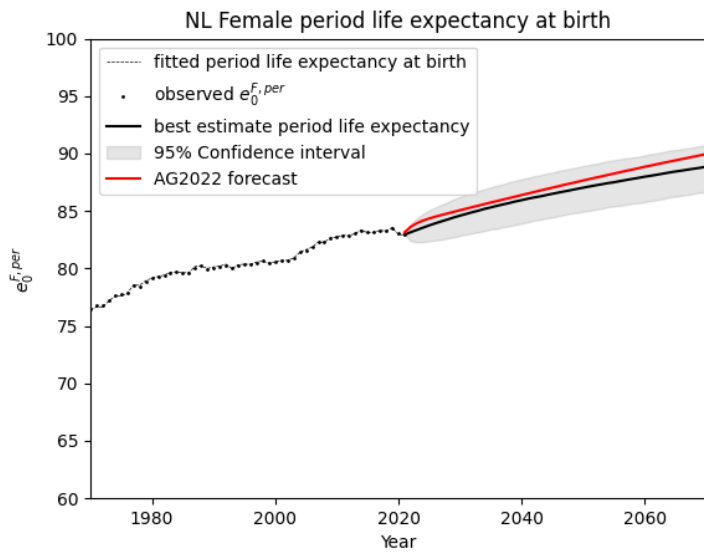


Figure 5.17: Observed and fitted period life expectancy for females (left) and males (right), calibrated on the years 1970-2021 for ages 0-90, closed by Kannisto's method. Period life expectancy forecasts and a 95% confidence interval for the years 2022-2070 are added as well. The red reference line is the AG2022 period life expectancy forecast.

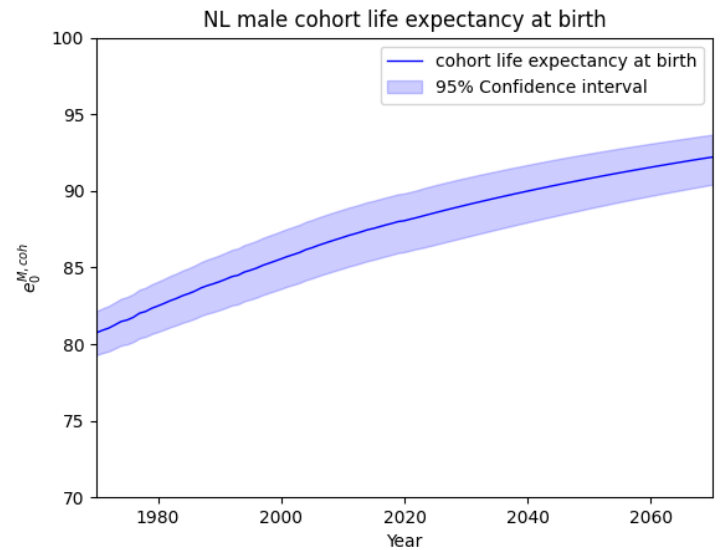
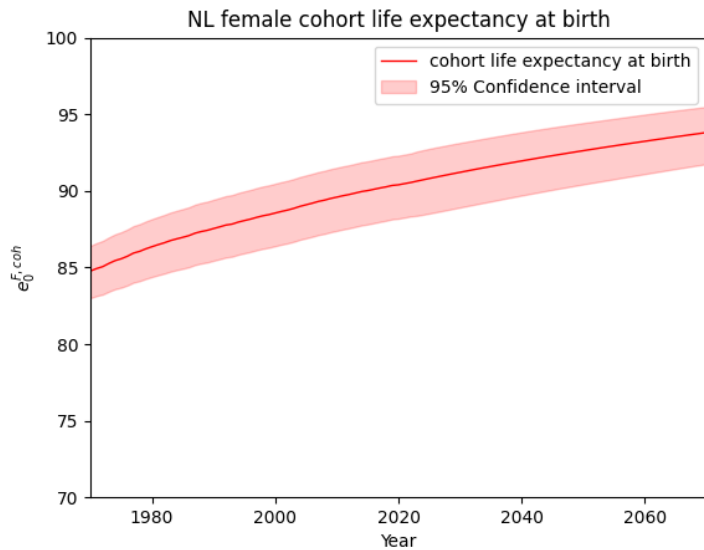


Figure 5.18: Fitted cohort life expectancy and its 95% confidence interval for females (left) and males(right), calibrated on the years 1970-2021 for ages 0-90, closed by Kannisto's method.

The best estimate period life expectancy is closer to the AG2022 forecast than in the benchmark model. Moreover, the confidence intervals are narrower compared to the confidence intervals in the benchmark model, particularly with

respect to the confidence interval for male period and cohort life expectancies. A possible explanation for the differences at high ages could be the usage of a different Kannisto approach by the AG2022 as described in 4.3.1. The Kannisto method used in the model incorporating mortality shocks, as described in 4.4.3, may have a dampening effect for high ages compared to the AG2022 model.

Lastly, Table 5.7 compares cohort life expectancies at birth between the benchmark model, the model from the sensitivity analysis, and the AG2022 model for the years 2024, 2045, and 2070.

Model	Starting year	Female	Male
Benchmark	2024	90.77	85.95
	2045	92.48	87.24
	2070	94.01	88.64
Sensitivity	2024	90.72	88.47
	2045	92.30	90.41
	2070	93.81	92.21
AG2022	2024	92.86	90.15
	2045	94.86	92.26
	2070	96.83	94.28

Table 5.7: Comparison of the cohort life expectancy at birth between the benchmark model, the model from the sensitivity analysis, and the AG2022 model for the years 2024, 2045, and 2070.

There is a significant difference between the cohort life expectancies at birth for males in the benchmark model and the model described in the sensitivity analysis. By calibrating data from 1970 onwards, instead of from 1900 onwards, the model yields higher estimates for male cohort life expectancies at birth in all future years. For females however, only minor differences in these numbers occur. The reason for this could be the inclusion of the many male deaths in the world wars when calibrating data from 1900 onwards. This inclusion could lead to an underestimation of cohort life expectancy. Excluding the two world wars, by calibrating data from 1970 onwards, results in higher male cohort life expectancies. However, the model still deviates from the AG2022 forecasts for cohort life expectancies for both genders. This discrepancy arises because the AG2022 sees Covid-19 as a disappearing trend in mortality, only affecting period life expectancies, and not including any other jump process. In contrast, the multi-population model incorporating mortality shocks also takes mortality jumps from the calibrated years into account. The probability and distribution of these jumps are simulated forward, causing potential mortality shocks into the future. This dynamic approach results in lower (cohort) life expectancies.

6 Conclusion

This thesis aims to incorporate mortality shocks into a multi-population mortality model. Historic events, such as the first World War, the second World War, the Influenza pandemic in 1918, but also the very recent Covid-19 pandemic, caused mortality shocks globally. Current mortality models, as employed by actuarial associations like the AG in the Netherlands, used to ignore these mortality shocks. This oversight leads to wrong forecasts for life expectancy and poses challenges for pension funds and life insurers in valuing their liabilities. By investigating the number of European deaths in 2020 and 2021, I find that excess mortality has occurred due to the Covid-19 pandemic. Many mortality models fail to incorporate these mortality shocks.

In this thesis, Using the Li-Lee model as a basis, similar to the models the AG employ, jump events are added to account for mortality shocks. The model is calibrated for ages 0-90 in the calibration period 1900-2021 using data on deaths and exposures from several (Western) European countries with similar GDP as the Netherlands. After parameter estimation, time-series models including a jump component, are used to produce mortality forecasts.

Additionally, an outlier analysis is conducted to observe any outliers in the mortality trend of the European reference group. In this outlier analysis, outliers during the years of the two world wars, during the Influenza pandemic, and during the Covid-19 pandemic are identified.

After parameter calibration for the time series, used for forecasting mortality rates, Kannisto is used for the closure of the mortality table. Having obtained estimates for the force of mortality for ages 0-120, forecasts can be made for period and cohort life expectancies. Compared to the AG2022 model, the multi-population model incorporating shocks projects lower period and cohort life expectancies. The transitory effect of the Covid-19 pandemic, as modeled by the AG, without considering the potential for future shocks could be a reason for this.

When altering the calibration period from 1900-2021 to 1970-2021, especially the male period and cohort life expectancies increase. Omitting the world wars in the calibration period, during which male mortality rates exceeded female mortality rates, resulted in these increased life expectancies. The choice of the calibration period plays a crucial role in capturing the impact of historical events on mortality trends. Using the calibration period from 1900 onwards, lead to more pessimistic life expectancies compared to the forecasts modeled by the AG. This raises the question whether large mortality shocks, such as the world wars or the influenza pandemic, will occur in the future. While

hoping for their absence, one can never be completely certain. Therefore, it is important to be prepared for such occurrences.

7 Recommendations

Several models incorporating mortality shocks exist, including regime switching models or models applying extreme value theory. Recommendations for future research include, instead of adding jumps, using regime switching models or extreme value theory to model shocks in a multi-population model. The existing literature focuses mainly on single-population models.

Moreover, the AG2022 model applies a different Kannisto extrapolation method compared to the one applied in this thesis. Instead of increasing death probabilities for high ages, the observed trend suggest that death probabilities should be decreasing for high ages. The new Kannisto method, as applied by the AG2022 model, could be a topic for future research when incorporating mortality shocks into a multi-population mortality model.

Additionally, future research may include investigating correlation between mortality shocks. Instead of assuming that mortality shocks are uncorrelated, a recommendation is to investigate what would happen with the model and its forecasts when incorporating correlated mortality shocks into a multi-population mortality model.

Lastly, altering the calibration period and assessing its impact on the parameter estimation and on the death probabilities is a crucial aspect for further research. Different calibration periods could have different projections for period and cohort life expectancies. The impact of the Covid-19 pandemic on mortality rates and life expectancy remains uncertain due to the lack of data and the ongoing evolution of the Coronavirus. As time progresses and more data becomes available, a more comprehensive understanding of the pandemic can be developed. With this additional information and data, more accurate forecasts for mortality and life expectancy can be generated.

Bibliography

- AG (2020). Prognosetafel 2020 Koninklijk Actuarieel Genootschap. Available online at: <https://www.actuarieelgenootschap.nl/kennisbank/projections-life-table-ag2020.htm> Accessed on 28 november 2023.
- AG (2022). Prognosetafel 2022 Koninklijk Actuarieel Genootschap. Available online at: <https://www.actuarieelgenootschap.nl/kennisbank/prognosetafel-ag2022-2.htm>. Accessed on 27 September 2023.
- Brouhns, N., Denuit, M., and Vermunt, J. K. (2002). A poisson log-bilinear regression approach to the construction of projected lifetables. *Insurance: Mathematics and economics*, 31(3):373–393.
- Chen, H. and Cox, S. H. (2009). Modeling mortality with jumps: Applications to mortality securitization. *Journal of Risk and Insurance*, 76(3):727–751.
- Chen, H. and Cummins, J. D. (2010). Longevity bond premiums: The extreme value approach and risk cubic pricing. *Insurance: Mathematics and Economics*, 46(1):150–161.
- CMI (2023). CMI Mortality Projections Model: CMI 2022. *CMI Working Papers*, 177.
- Cox, S. H., Lin, Y., and Wang, S. (2006). Multivariate exponential tilting and pricing implications for mortality securitization. *Journal of Risk and Insurance*, 73(4):719–736.
- EUROS (2023). Eurostat. Data available at <https://ec.europa.eu/eurostat>. (data downloaded on 06-11-2023).
- HMD (2023). HMD. Human Mortality Database. Max Planck Institute for Demographic Research (Germany), University of California, Berkeley (USA), and French Institute for Demographic Studies (France). Available at www.mortality.org (data downloaded on 06-11-2023).
- Kannisto, V. (1992). *Development of the oldest – old mortality, 1950-1980: evidence from 28 developed countries*. Odense University Press.
- Kendall, M. and Ord, J. (1990). *Time Series*. Edward Arnold.
- Lee, R. D. and Carter, L. R. (1992). Modeling and forecasting us mortality. *Journal of the American statistical association*, 87(419):659–671.

- Li, N. and Lee, R. (2005). Coherent mortality forecasts for a group of populations: An extension of the lee-carter method. *Demography*, 42:575–594.
- Lin, Y. and Cox, S. H. (2008). Securitization of catastrophe mortality risks. *Insurance: Mathematics and Economics*, 42(2):628–637.
- Melenberg, B. (2021). 2021lectures macro longevity risk. Lecture notes Life Insurance, 2021. Tilburg University.
- Milidonis, A., Lin, Y., and Cox, S. H. (2011). Mortality regimes and pricing. *North American Actuarial Journal*, 15(2):266–289.
- Renshaw, A. E. and Haberman, S. (2006). A cohort-based extension to the lee–carter model for mortality reduction factors. *Insurance: Mathematics and economics*, 38(3):556–570.
- Statistics Netherlands (2023). Levensverwachting; geslacht; leeftijd. “Results based on calculations by Statline using non-public microdata from Statistics Netherlands.”
- Wilmoth, J. R., Andreev, K., Jdanov, D., Gleijeses, D. A., Boe, C., Bubenheim, M., Philipov, D., Shkolnikov, V., and Vachon, P. (2007). Methods protocol for the human mortality database. *University of California, Berkeley, and Max Planck Institute for Demographic Research, Rostock*. URL: <http://mortality.org> [version 31/05/2007], 9:10–11.

A Appendix

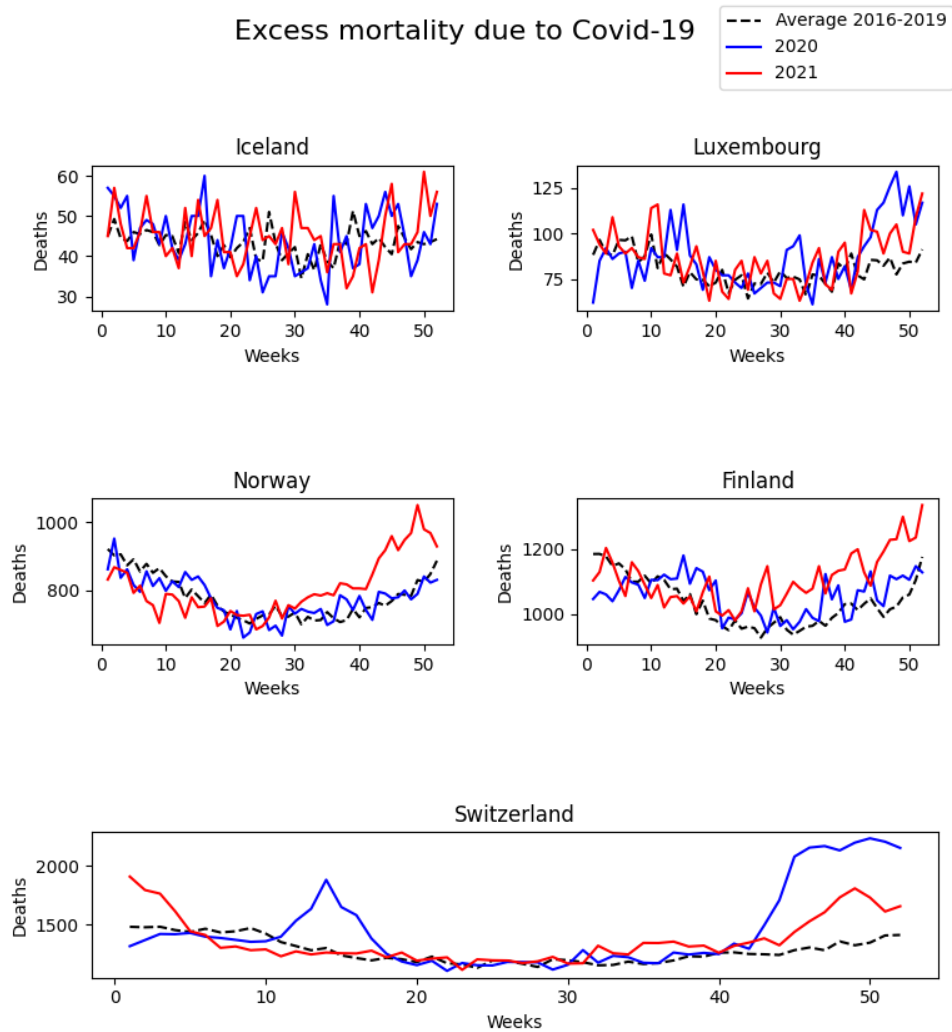


Figure A.1: Excess deaths in Iceland, Luxembourg, Norway, Finland, and Switzerland during the Covid-19 pandemic. The graphs represent the number of deaths per week in 2020 and 2021 compared to the average deaths per week in 2016-2019. Source: STMF (2023)

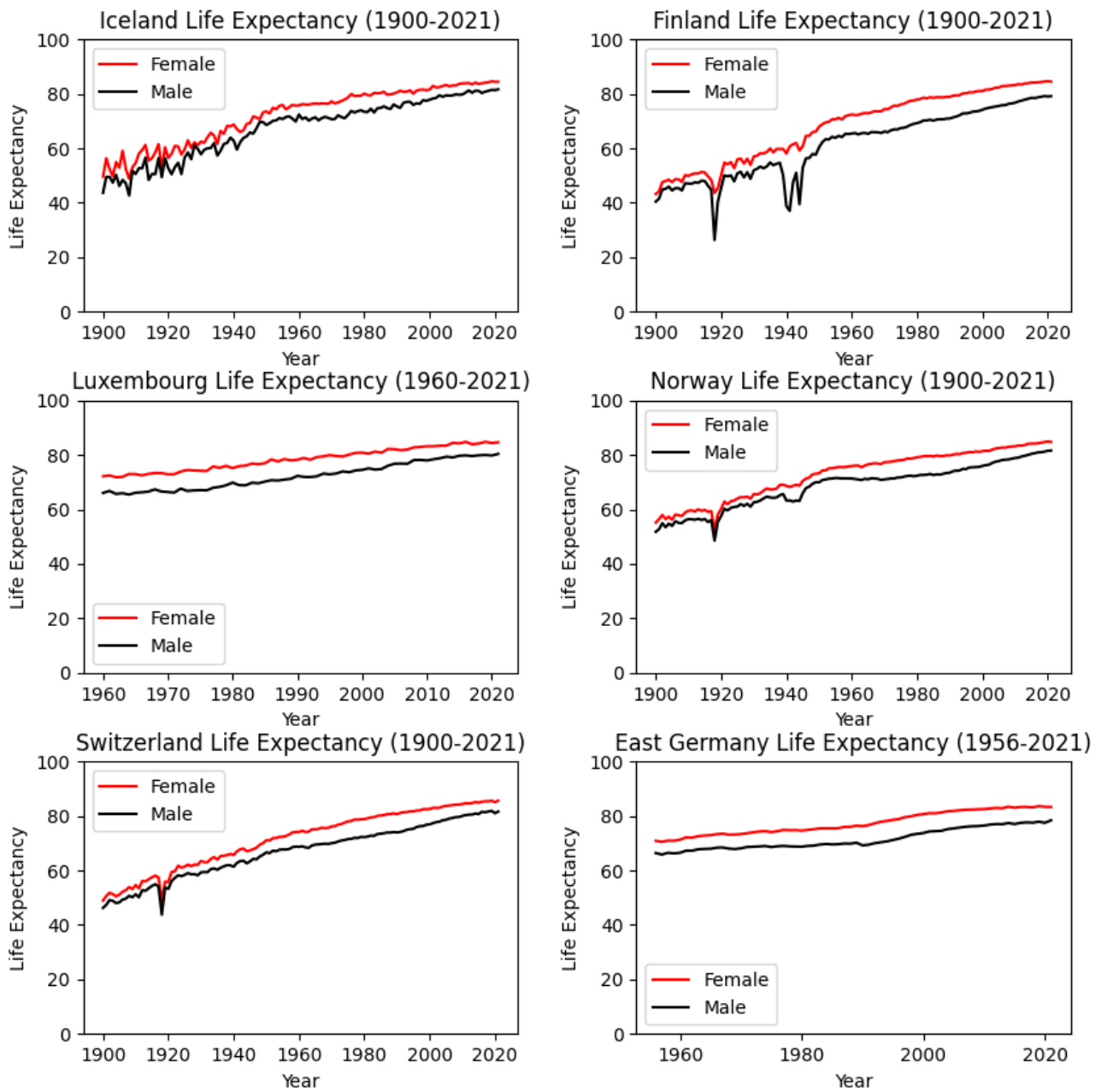


Figure A.2: The evolution of male and female period life expectancy in Iceland, Finland, Luxembourg, Norway, Switzerland, and East-Germany for different time periods. Source: HMD (2023)

Country	1900-2018	2019	2020	2021
Austria	HMD	HMD	EUROS	EUROS
Belgium	HMD	HMD	HMD	HMD
Denmark	HMD	HMD	HMD	HMD
Finland	HMD	HMD	HMD	HMD
France (Metropolitan)	HMD	HMD	HMD	HMD
Germany	HMD	HMD	HMD	EUROS
Iceland	HMD	HMD	HMD	HMD
Ireland	HMD	HMD	HMD	EUROS
Luxembourg	HMD	HMD	HMD	HMD
Norway	HMD	HMD	HMD	HMD
The Netherlands	HMD	HMD	HMD	HMD
Sweden	HMD	HMD	HMD	HMD
Switzerland	HMD	HMD	HMD	HMD

Table A.1: Data sources for each country in each year of the calibration period. Data from the years 1900-2018 all are obtained from the HMD.

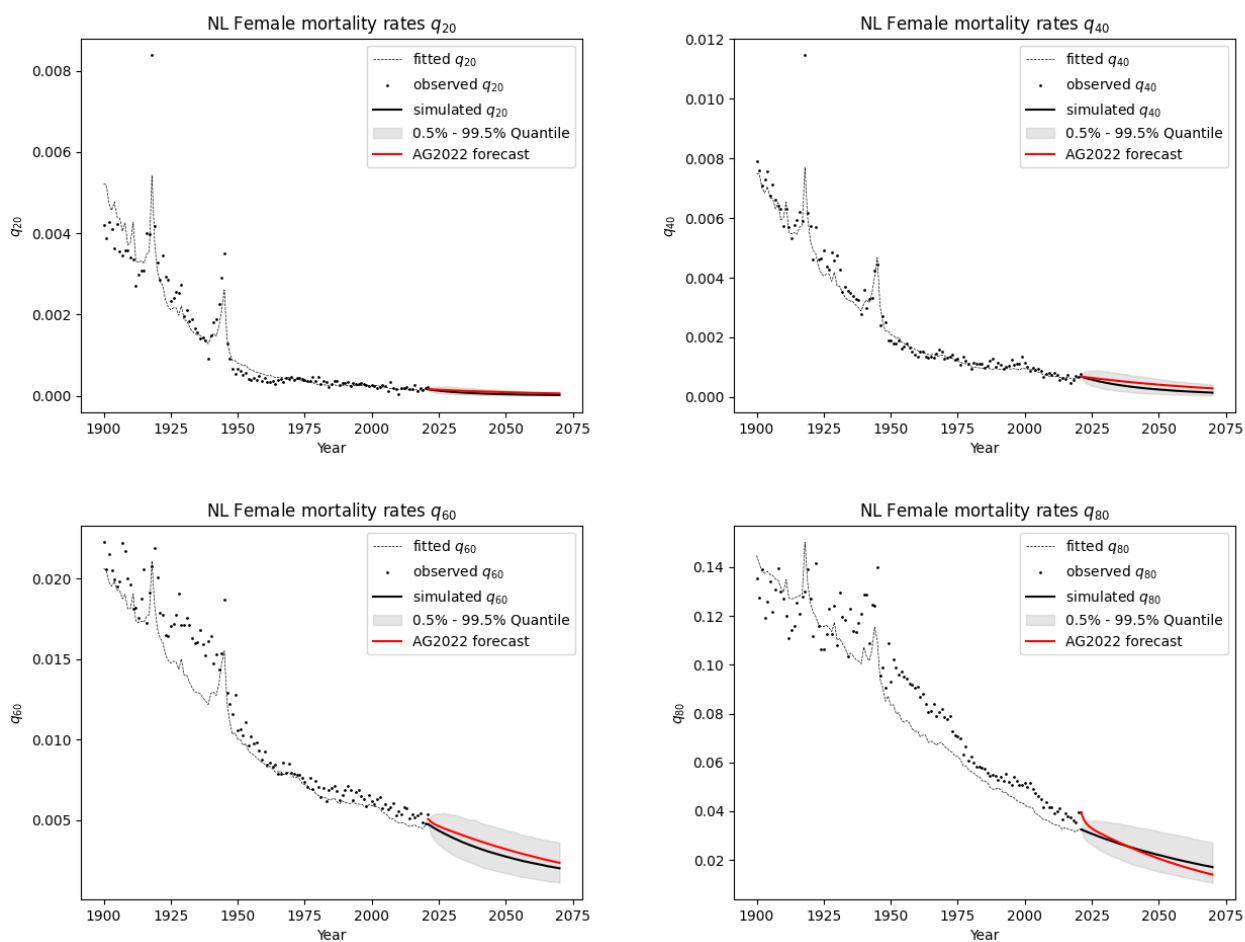


Figure A.3: Estimates, observed values, and forecasts for death probabilities for ages 20, 40, 60, and 80 for Dutch females. Calibration period 1900-2021, and projection 2022-2070. The median and the 99% confidence interval obtained from 10,000 simulations are plotted. As a reference, the AG2022 forecast is added as well.

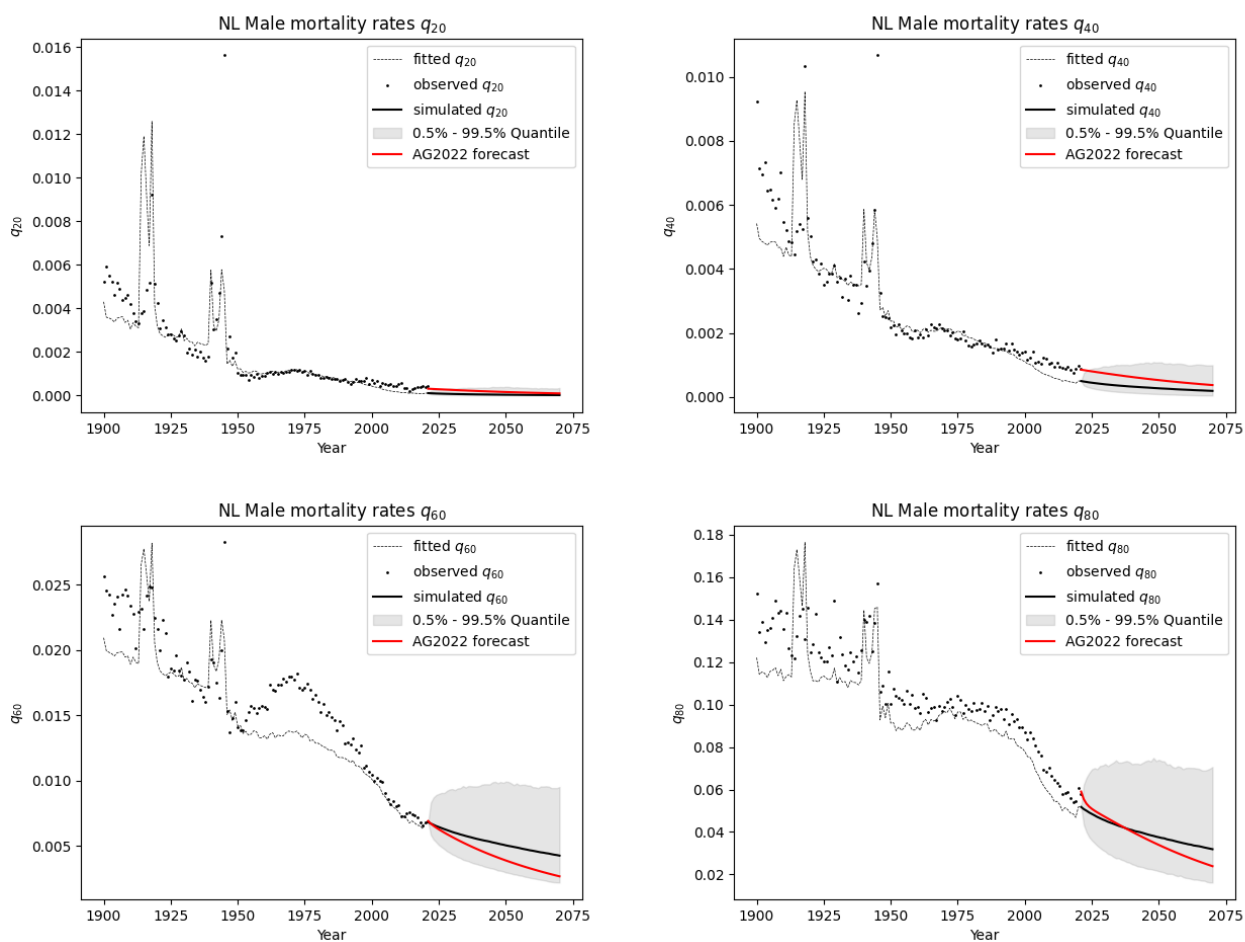


Figure A.4: Estimates, observed values, and forecasts for death probabilities for ages 20, 40, 60, and 80 for Dutch males. Calibration period 1900-2021, and projection 2022-2070. The median and the 99% confidence interval obtained from 10,000 simulations are plotted. As a reference, the AG2022 forecast is added as well.

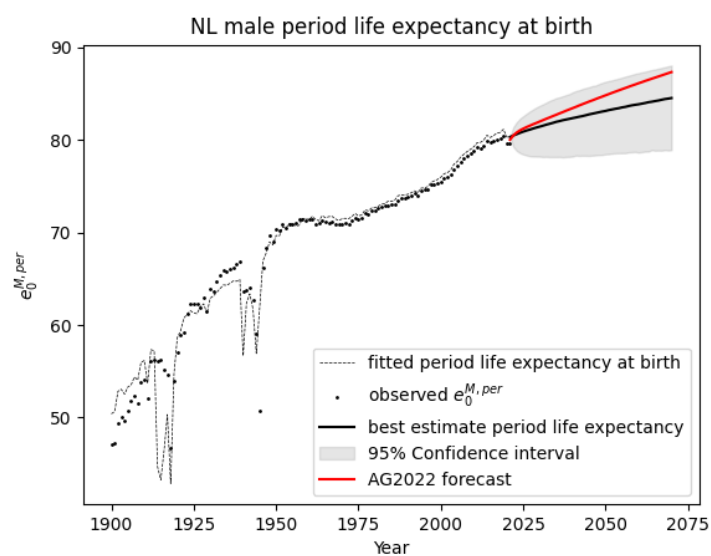
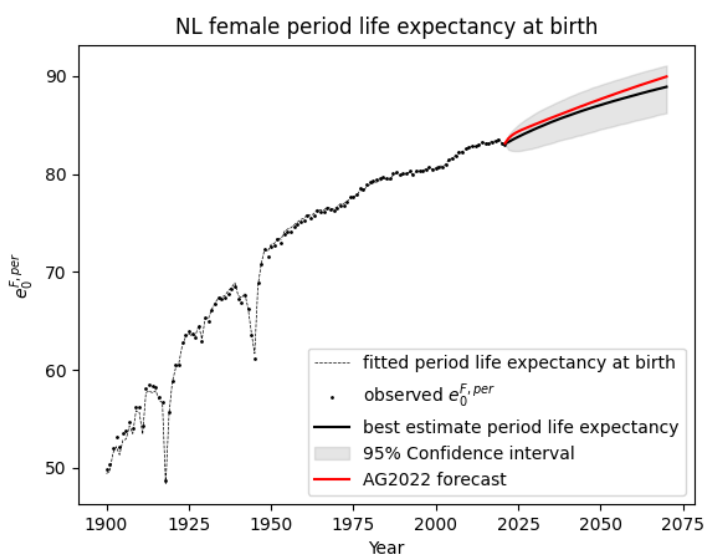


Figure A.5: Observed and fitted period life expectancy for females (left) and males (right), calibrated on the years 1900-2021 for ages 0-90, closed by Kannisto's method. Period life expectancy forecasts and a 95% confidence interval for the years 2022-2070 are added as well. The red reference line is the AG2022 period life expectancy forecast.

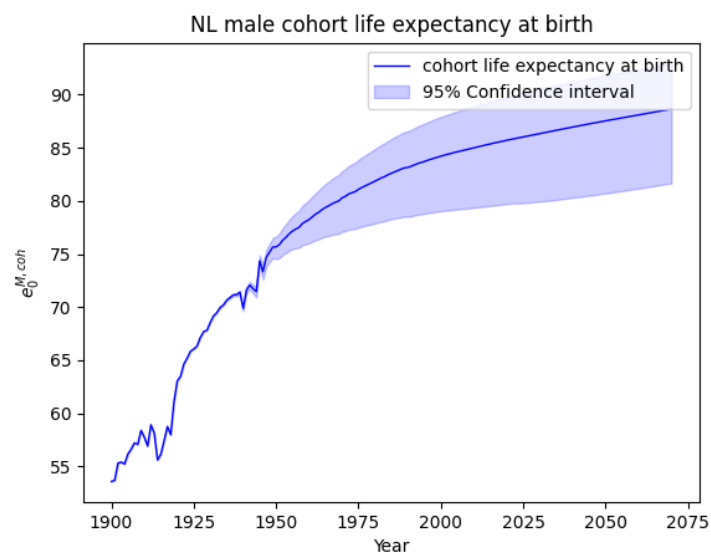
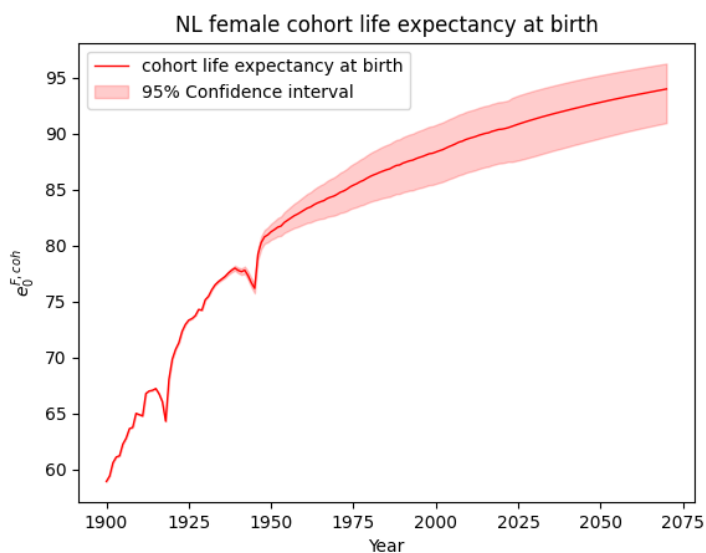


Figure A.6: Fitted cohort life expectancy and its 95% confidence interval for females (left) and males(right), calibrated on the years 1900-2021 for ages 0-90, closed by Kannisto's method.